Characterizing the style, composition, and timing of Cedar River Landslide Complex

Sarah Polster

A report prepared in partial fulfillment of
the requirements for the degree of

Master of Science
Earth and Space Sciences: Applied Geosciences

University of Washington

March 2017

Internship coordinator:
Kathy Troost

Reading committee:
Juliet Crider
Kathy Troost
Alison Duvall

Project mentor:
Bruce Stoker, Earth Systems

MESSAGe Technical Report Number: 051

1.0 Executive Summary

The Cedar River Landslide Complex (CRLC) is a series of debris flowslides about 3 km down river from the Masonry Dam at Chester Morse Reservoir in the Cedar River Municipal Watershed, the source of drinking water for 1.4 million people in Seattle, WA. These hillslope failures all originated from the terminal moraine deposits of the Puget lobe of the Vashon glacier. The CRLC was discovered in 2009 by new geologic mapping and LiDAR imagery.

This study created a landslide inventory, including dimensions, composition and dating all units of the CRLC. Fieldwork involved digging test pits at sites on three different units of the CRLC. Soil samples of all units, including both landslide and undisturbed material were collected. Sieve analysis tests, water content, and mineralogy data were collected. Volumes of each unit of the CRLC were calculated to determine mobility indices for each landslide to compare the CRLC to other large landslides in the region. To estimate the ages of the CRLC slides, radiocarbon samples were collected and surface roughness of the landscape was calculated using GIS.

The underlying material in the Cedar River valley is well-graded gravel and the CRLC is composed mostly of well-graded gravel and sand. The landslide material has lower water content than the underlying material.

Five absolute dates on three landslides were calculated using radiocarbon dating. The dated CRLC slides range in age from 170 Yr B.P. to younger than 6,850 Yr B.P. Standard deviation of slope (SDS) was used as a measure of surface roughness, the roughness of the CRLC has a small range in values (4.15 to 4.51°). No correlation between surface roughness and landslide age was found. Several reasons for this are discussed. No correlation suggests the surface roughness measure used in this study (standard deviation of slope) is not a good measure of landslide age in this watershed. Absolute ages are calculated using organic samples found in soil horizons below the landslide material. As such, these dates represent only the maximum age and may not accurately date the events.

A series of landslide triggers are considered, including coseismic, glacial retreat, and precipitation events, however our dataset does not allow definitive conclusions or elimination of any particular trigger. Future work, including gathering more samples for landslide ages, is needed to consider the full landslide history of this complex.

1.0 Introduction

The Cedar River Landslide Complex (CRLC), is a series of debris flowslides (Hungr et al., 2014) recently discovered in the valley of the Cedar River near North Bend, Washington (Fig. 1). Not visible in aerial photography due to heavy vegetation (Fig. 1), the CRLC was discovered only recently using light detection and ranging (LiDAR) imagery. Originally mapped as a smaller unit of three flows (Dragovich et al., 2009), the CRLC has been dramatically enlarged to nine flows with recent LiDAR imagery by King County geologists and Seattle Public Utilities (Stoker, 2016; PSLC, 2014). This study aims to characterize this landform and place the debris flows into a larger regional context.

In the Pacific Northwest, recent landslides have brought attention to the potential to affect human lives and infrastructure. The Oso landslide, located 60 miles north of CRLC in the North Fork of the Stillaguamish River (NFSR; officially known as the SR 530 Landslide) was one of the largest landslides in Washington and United States' history (Keaton et al., 2014). Although a different type of slope failure, the CRLC shares some characteristics with the Oso and both landforms originated in glacial sediments (Riemer et al., 2015).

Located in the City of Seattle's Cedar River Municipal Watershed between Chester Morse Reservoir and the diversion dam at Landsburg, the CRLC is a prominent feature in the river valley and of concern to the Seattle Public Utilities (SPU; Fig. 2). The Watershed, owned by the City of Seattle, is the source of drinking water for 1.4 million people in the greater Seattle area (Seattle Public Utilities, 2016). Three of the CRLC debris flows cross the river (Fig. 1), suggesting future events could block or dam the river. Sediment entering the river increases turbidity of drinking water downstream at the Landsburg water intake, leading to concerns to public health, including gastrointestinal diseases (Mann et al 2007).

Creating a landslide inventory for the area allows for future slope stability, landslide distribution and statistics, and landscape evolution studies (Guzzeti et al., 2012). This study aims to characterize the morphology, composition and timing of the CRLC and to compare these flowslides to other large events in the region and worldwide.

2.0 Background

The morphology of these slide deposits is consistent with the mechanics of debris flowslides, which are rapid flows characterized by excess pore-pressure usually originating in several retrogressive failures (Hungr et al, 2014). At this site, the flowslides originated from moderately steep (about 35°) slopes of Seventeen Creek Ice Contact Complex, which is a morainal complex (SCICC; Dragovich et al., 2009) (Fig. 3). The numbering system used in this report originates from and is consistent with a report by Stoker (2016) that catalogs all active landforms in the Watershed (Fig. 4).

While no previous work has been undertaken on the CRLC or SCICC, extensive work has been conducted upriver related to failures and landslides that occurred as a result of the partial filling of the Chester Morse reservoir (Fig. 2). This dam has had problems related to permeability and seepage since the year it was constructed in 1918 (Mackin, 1941; Landau Associates, 2006).

The original dam on the Cedar River was built in 1904, and enlarged in 1918. On December 23, 1918, an outburst flood originating from the embankment, entered the Snoqualmie valley destroying the small town of Edgewick, Washington. The failure was interpreted by Mackin (1941) to have been caused by a buildup of hydrostatic pressure in the gravels of the morainal embankment, caused by rising water levels in the reservoir. Groundwater in the embankment varies in elevation with reservoir levels (Landau Associates, 2006). Approximately 1/3 of the embankment's elevation relates to isostatic rebound following ice retreat (Thorson, 1981). Seepage from the newly created Chester Morse Lake reservoir through the embankment deposit also inundated the small railroad town of Moncton that is now Rattlesnake Lake (Fig. 5).

Anthropogenic forces have affected the topography of the Cedar River for over 100 years. The Cedar River Watershed has been owned by the City of Seattle since 1900. The area was actively logged and mined until the 1930's and several railroads traversed the area from 1882 until 1992 (Cedar River Municipal Watershed 2013). Due to declining populations of chinook salmon, Seattle developed a Habitat Conservation Plan in 1993. This plan limits access to the watershed and determines management decisions (City of Seattle, 2000).

2.1 Geologic Setting

As the Puget Lobe of the Frasier glaciation advanced into the Puget Lowland approximately 17,500 years ago, rivers flowing west from the Cascade Mountains were temporarily dammed by glacial ice (Mackin, 1941; Porter and Swanson 1998; Dragovich et al., 2009). At the terminus of the glacier, an embankment of moraine material accumulated. One such embankment composed of glaciofluvial deltaic material is deposited across the Cedar River valley (Mackin, 1941; Booth, 1986).

Two recessional outwash deposits, Seventeen Creek Ice Contact Complex (SCICC) and the Cedar Kame Terrace (Dragovich et al 2009) are directly upslope of the CRLC and the source area of the landslides (Fig. 3). SCICC is a unit of the morainal embankment and represents the terminal edge of the Puget lobe (Frizzel et al., 1984; Booth, 1986; Mackin, 1941). The embankment is dominated by bedded gravels and sands that represent recessional outwash into ice proximal lakes (Booth, 1986).

Within a few kilometers of the CRLC, the valley is crossed by several active faults. The Rattlesnake Mountain Fault Zone (RMFZ) is a series of at least 11 northeast-dipping, strike-slip faults that appear to be an extension of the South Whidbey Island Fault Zone (SWIF) and cross the Cedar River valley 1 mile upriver from CRLC (Dragovich et al. 2009). The RMFZ intersects with the Steele Creek fault. Deformed Vashon advance lake deposits in the Snoqualmie River valley suggest movement in the fault zone since the last glacial advance. Rattlesnake Mountain Fault strand RMFZ-6 or RMFZ-11 are the suspected source(s) of a moderate earthquake (M5.5-5.7) near Chester Morse Lake (Fig. 2) that occurred on April 29, 1945 (Dragovich et al., 2009). Due to lack of exposure, Dragovich et al. (2009) were unable to discern any Holocene offset along RMFZ, although a cluster of earthquake hypocenters might imply recent movement. This lineament is surrounded by a series of folds, that are expressed at the Cedar River by the Lindsey syncline, whose axis passes below Landslide 28 in the CRLC (Fig. 3).

Geologic mapping indicates the sediments in the valley floor are a mix of modern fluvial deposits and Vashon glacial outwash (Dragovich et al., 2009). Unlike the neighboring South and Middle forks of the Snoqualmie River, the Cedar River has not incised a deep channel through the embankment (Mackin, 1941) but rather was forced over the volcanic bedrock on the south side of the embankment forming the Cedar Canyon.

2.2 Precipitation

The climate of the area in and immediately surrounding a landslide complex can be an important factor in determining failure causes. At Chester Morse Reservoir, the average annual precipitation is 97.39 inches. For comparison, the Darrington Ranger Station, the closest station to Oso, has an average annual precipitation of 75.96 inches (Arguez et al., 2012). The Köppen-Geiger climate classification for Cedar River Watershed is Csa, which denotes warm climate with hot and dry summers (Kottek et al., 2006). Oso, 60 miles to the north, has a Ctb climate; warm temperature, fully humid hot temperature summers (Keaton et al., 2014). Both sites are located on the western flank of the Cascades, where the highest rates of precipitation occur between late fall and early winter (Henn et al., 2015).

3.0 Methods

Data were collected on the material composition of underlying lithologic units, the landslides were mapped and their area and volume dimensions calculated, and samples were collected for radiocarbon dating to estimate failure age as part of a new detailed inventory and characterization of the CRLC. The detailed methodology of each objective is listed in the subsections below.

3.1 Digital Mapping and Groundtruthing

Stoker (2016) originally mapped the CRLC digitally using 3m resolution bare-earth LiDAR images. Some smaller units (landform 32 and 23 Fig. 4) are thought to be secondary remobilizations of larger failures, but are mapped as separate events (2016). In this study, the mapped flowslides were verified in the field by examining surface morphology and stratigraphy. Where discrepancies were found, polygons were redrawn. Fieldwork was conducted in November 2016. The City of Seattle generously donated the use of an extend-a-hoe and operator for one week. Site reconnaissance (undertaken in July 2016) and desk review determined sites of interest. Sites near the toes or levees of landslide were favored (Fig. 4). It was necessary for sites to be located near roads for backhoe access. Therefore, Landslide 28 became the focus of this study due to accessibility and good exposures. Landslide 28 could be accessed by road at several areas of interest, including the levees, toe, and head scarp. Trenching Site 8 was selected because in office review it appears flowslides 21 and 22 overlap. Crosscutting relationships were established between Landslides 22 and 21 at this site trench.

A test pit was opened and excavated in increments at locations accessible by the backhoe and undisturbed by road building (where possible). Samples were collected with each change in lithology observed. The depth of each pit varied, depending on the units and soil horizons found. The top of each soil horizon was inspected for organic material, representing the last growth before burial by the slide deposit. Test pits was logged and documented with

sketches and photographs. Site descriptions are compiled in Appendix B. Depths of landslide materials were measured using tape measures in open pits.

3.1.1 Ground Penetrating Radar

A Ground Penetrating Radar (GPR) survey was conducted by Washington Department of Natural Resources (DNR) geologists Kara Jacobacci and Trevor Contreras in tandem with our fieldwork. The goal was to discern the thickness of the flowslide and investigate the "bench" feature found near the crown of most of the CRLC (Fig. 6).

3.2 Composition or Index Properties

Index properties, such as grain size, mineralogy and water content, influence the residual strength of the soil (Wen et al., 2003). Changes in material properties can lead to changes in mobility. When saturated, finer grain sizes can increase the velocity and pore pressure of a debris flow (Wang and Sassa, 2003). These index properties are used for quantitative comparison between soils (Wen et al., 2003).

To better identify landslide materials, soil samples were collected in both the native or undisturbed material nearby or buried by the slides and from the landslide-transported material (Fig. 4). Index property testing was conducted 1-2 weeks after samples were collected in the field and dried in an oven.

3.2.1 Grain size distribution

Gradation curves illustrating grain size distribution for each sample collected were created using sieve methods, as described in ASTM D422-63 (2007): Standard Test Method for Particle-Size Analysis of Soils (http://astm.org/). Most samples had very few fines, so no hydrometer testing was conducted. Largest grain sizes of each deposit were recorded in the field and during sieve analysis for samples too large for available sieves. Detailed results are presented in Appendix A.

3.2.2 USCS Designation

The results of the grain size analysis were used to assign Unified Soil Classification System (USCS) soil classifications following ASTM D2487-11 - Standard Practice for Classification of Soils for Engineering Purposes (Unified Soil Classification System) (http://www.astm.org/). Designations are listed in Appendix A.

3.2.3 Water Content

Determination of the water content (w), defined as the ratio of the mass of water relative to the mass of solids in a given volume of soil, is guided by ASTM D2216-10 - Standard Test Methods for Laboratory Determination of Water (Moisture) Content of Soil and Rock by Mass (http://www.astm.org/). Samples were weighed and placed in an oven overnight in a laboratory at the University of Washington. The next day, samples were weighed again and the difference in weights is the original water content of the sample.

Water content was measured and recorded for those materials that were transported and stored in a sealed condition in plastic freezer bags. This provides confidence that the materials did not dry out between the time of sampling and testing in the laboratory several

days later. However, some bags were not sealed properly. Conditions during collection were not ideal: most samples were collected during a precipitation event that lasted several days. I suspect near surface samples were saturated by the storm; thus, water content values could be more representative of wet season conditions.

3.2.4 Mineralogy

Previous authors have established that the Cedar River embankment was deposited at the terminal moraine of the Puget Lobe (Dragovich et al., 2009; Mackin, 1941). The morainal embankment including green metamorphosed igneous rocks sourced on the flanks of Mount Si, with no source in the Cedar watershed (Mackin, 1941). Determining the provenance of sedimentshelps determine which glacial unit the landslide originated from based on an analysis conducted by Landau Associates (2006). Results are compiled in Appendix C.

3.3 Landslide Dimensions

The area of the CRLC units were calculated from the mapped GIS polygons using the Spatial Analyst tool. Understanding the amount of material in a mass wasting event allows direct comparison to other large events. However, determining the volume of a landslide is not a straightforward task. Two methods strategies were used to calculate area: 1) a maximum value was calculated by multiplying the surface area of each slide by depths measured in the field. This value is considered a maximum because this calculation assumes a rectangular shape of material and not all units were measured, so a second value was necessary. 2) An empirical relationship between surface area and volume calculated by previous authors (Larsen et al., 2010; Hovius et al., 1997; Guzzeti et al., 2009) utilize a relationship between surface area and volume to calculate volumes quickly and remotely. The relationship presented by Guzzeti et al. (2008) is:

$$V_L = 0.074 \times A_L^{\alpha} \quad (1)$$

where V_L is the landslide volume (m^3), A_L is landslide area (m^2) and α is a scaling factor. Guzzeti et al. (2010) uses 1.450 as a value for α, but Larsen and Montgomery (2010) caution that this value may be dependent on landslide size and materials. As the CRLC are relatively small and soil (as opposed to bedrock), 1.450 is used in this study.

3.4 Landslide Mobility Indices

Understanding the factors controlling mobility and runout of large events can contribute to the ability of predicting hazards (Dade and Huppert, 1998). I use field-based depth measurements and flowslide dimensions extracted from GIS maps to calculate three different mobility indices; the L/H ratio, the $A/V^{2/3}$ratio, and the radial spread index, R_S.

The L/H ratio (length/height) of a landslide is the oldest and most widely used measurement index for mobility (Iverson et al., 2015). H is defined as the elevation difference between the top of the head scarp and the toe of the deposit. L is defined as the length from the head scarp to the edge of landslide toe (Hsu, 1978).

A second mobility index is the ratio $A/V^{2/3}$, where A is planimetric area of a landslide path, and V is landslide volume (Griswold and Iverson, 2008). By excluding H, this index

accounts for effects of topography that channelizes runout (Iverson et al., 2015). GIS was used to calculate surface area of each flowslide.

As a landslide travels downhill and new material is entrained, the resulting change in volume affects the coefficient of friction. Therefore, a third index of mobility, R_S, accounts for these changes (Dade and Huppert, 1998). This index aims to account for the potential energy of the landslide, but requires very little spreading to be accurate (Iverson et al., 2015):

$$R_S = \rho g V H \quad (2)$$

where g is acceleration due to gravity, ρ is bulk density of material (Dade and Huppert, 1998).

Density was determined using the relationship between seismic velocities and density

$$\rho = 8.32 \cdot \log(V_S) - \log(depth) \quad (3)$$

where ρ in kN/m^3 is the in-situ unit weight, V_s (m/s) is the seismic velocity. Using the seismic velocities and depths (Appendix D) from the geologic model of Landau Associates (2006), densities of the native materials are calculated. Average densities of native materials measured in Landau Associates (2006) were substituted as density for flowslide material.

3.5 Landslide Age Analysis

Landslide hazard is the probability of a damaging event in a given area (Varnes, 1978) and as such, landslide frequency is an important component of landslide inventories (Bell et al., 2012).

3.5.1 Absolute Ages

Radiocarbon dates of charcoal and woody debris found at 6 sites were used to obtain absolute ages of Landslides 21, 28 and 30 (Fig. 4). All wood samples were analyzed at DirectAMS in Bothell, WA and one sample was analyzed at Beta Analytics in Miami, FL. Volcanic ash discovered in the pit at site 8 (Fig. 4) was sent to the GeoAnalytical lab at Washington State University to identify provenance and age of the volcanic material. The ash, found in the soil horizon below landslide material is also considered a maximum age for the landslide event.

Radiocarbon samples were collected within excavated trenches from the top layers of soil horizons directly underlying the landslide deposits. Wood and ash samples are interpreted to have been living before the flowslide event and represent the maximum age of the event.

3.5.2 Surface Roughness

Surface roughness provides a quantifiable measure of surface morphology and has long been used as an indicator of relative age of a geomorphic feature. After creating an initial rough surface, diffusional soil creep processes tend to smooth features and decrease roughness elements, such as hummocky landslide topography, over time (Booth et al., *in press*).

Unlike the main body of a landslide, head scarps have smooth surfaces and become rougher over time (Grohmann et al., 2010). To compare the roughness of only slide deposits, all visible head scarps were removed from mapped polygons, as per the methodology of LaHusen et al. (2016) and Booth et al. (*in press*).

Disturbed or human altered areas were also removed from surface roughness analysis with a 10m buffer where possible. Gully features identified in the LiDAR were also removed from flowslides, as per (Booth et al., *in press*; LaHusen et al., 2016).

Surface roughness was quantified using Standard Deviation of Slope (SDS) because it captures sudden changes in slope and is best suited for steep slopes (Grohmann et al., 2010). The average standard deviation of slope (SDS) within a 3 x 3 cell was found to be correct for 87% of landslides in NFSR (Booth et al., *in press*). Other methods to quantify surface roughness include wavelet functions (Booth et al., *in press*) and vector dispersion (Grohmann et al., 2010), but the simpler methods have been found to show better results than the more complex methods (Berti et al., 2013).

The highest values for surface roughness on a landslide tend to group around levees and toes (Glenn et al., 2006). Especially on debris flows, where high shear stresses cause a decrease in friction angle as the mass moves (Hungr, 2007). Average surface roughness values were calculated over the entire slide mass as well as by isolating only toes and levees in order to account for this.

4.0 Results

4.1 Digital Mapping and Ground Truthing

Nine flowslides were remotely mapped in the CRLC. However, one (Slide 24) was eliminated after intact glacial till was discovered at the surface during fieldwork (Troost per comm, 2016). All larger units of the CRLC show very little lateral spreading (Fig. 4). Three flowslides (30, 28, and 21) cross the Cedar River.

4.1.1 Ground Penetrating Radar

Radargrams of the survey results show that Qls (flowslide material) has a chaotic internal stratigraphy and no rotated units. The portion interpreted as flowslide is in yellow on the radargrams. Several radargrams show horizontal or subhorizontal reflectors (Fig. 7b). Most surveys were conducted on road surfaces, this disturbed area is indicated in purple on the radargrams (Fig. 7).

4.2 Material Composition

4.2.1 Index Properties

To identify flowslide material, I documented both undisturbed (native) and transported material (slide deposits). Results are summarized in the subsections below

4.2.1.1 Native, Undisturbed Materials

Samples of native material were collected at Sites 5 and 1 (Fig. 4; Full sample descriptions Appendix B). All samples were well graded and ranged from sand to gravel (Table

1). The uppermost units in both sites have water content over 20%, but transition to less than 10% in the lower units.

Table 1- Summary of properties of native material of Cedar River Valley. Unit 1-M was interpreted as colluvium and not included in this table. Units 5-UL and Unit 1-L are possibly interpreted as the same unit (Unit 2 in Landau Associates, 2006).

Properties of Native Material							
Sample	**Water content, w**	**C_U**	**C_C**	**USCS**	**Description**	**Field Hardness**	**Interpretation (Landau 2006)**
5U	22.6	31.7	1.1	SW-SM	Well graded sand with silt and gravel	Loose to medium	Unit 1 or 2
5L	8.1	17.5	3.2	GW	Well graded gravel	Very hard	Unit 3
1L	5.9	7.5	0.7	SW	well graded sand with gravel	Loose	Unit 1 or 2

At site 1, two units were observed (Appendix B section 10.1). The upper sample was interpreted to be colluvium and is not described below. Sample 1L is a subangular to rounded greenish-gray well graded gravel (Fig. 8). This unit is weakly stratified and coarsens downward.

At site 5, an upper (5U) and lower (5L) unit were observed (Appendix B section 10.4). Unit 5U is loose to a medium dense sand with silt and gravel. The hardness of this unit suggests it corresponds with Unit 2 of Landau Associates (2006). Sample 5L is a very dense, well sorted sand with gravel (Fig. 8).

4.2.1.2 Flowslide Materials

The material of the CRLC is mostly coarse, well sorted gravel material (Fig. 8; Appendix B). Sample 2B was collected from the toe, 4B from the lateral levee and sample 7A from the main body of landform 28 (Fig. 4). Sample 10A was collected on the lateral levee of landslide 30 and sample 8B-2 was collected on the lateral levee of landform 21 (Fig. 4).

Table 2- Summary of index properties of materials collected from the CRLC. Samples were collected on three separate landforms and in all landslide zones (Fig. 5). Sieve results are compiled in Appendix A and site descriptions are compiled in Appendix B.

Properties of the CRLC						
Sample	**CRLC Unit**	**Water content in %, w**	**Cu**	**Cc**	**USCS**	**Description**
7A	28	2.6	8.3	0.9	GW	well graded gravel with sand
10A	30	9.1	35.6	1.7	GW	well graded gravel with sand
8B-2	21	4.7	18.8	0.5	SW	well graded sand with gravel
2B	28	5.1	26.7	5.9	GW	well graded gravel with sand
4B	28	24.8	47.5	0.5	SM	Silty sand

All samples (besides 4B) have low water contents (Table 2). Sample 7A is an oxidized, loose, well graded gravel with sand. Sample 2B is also a well graded gravel with sand.

Sample 10A is a loose, well graded gravel with sand. Sample 10A had cobbles and boulders throughout the deposit, as well as some loose stratification in the boulders near the top of the deposit and fined down column (Appendix 10.7).

Sample 4B has very different characteristics from the other CRLC samples (Table 2). 4B is primarily sand, whereas all other CRLC samples were primarily gravel. The coefficient of uniformity (C_u) value is erroneously high because the D_{10} value is underestimated due to smaller grain size. The smaller grain size could also account for the higher water content. The other sand sample (8B-2) also has a higher water content (9.1%).

4.2.4 Mineralogy

Materials from the flowslides contain more quartz and less granitic lithics than the underlying material. The flowslide material also contains red, weathered lithics. These lithics are not found in the native material below the slide deposits (Appendix C). A possible source of the red lithics is the Triassic bedrock cliffs above SCICC (Fig. 3; Stoker per comm, 2016).

4.3 Landslide Dimensions

4.3.2 Area and Volume Estimates

The area and volume of each flowslide was calculated using Eq. 1 and GIS polygons. The volume of the flowslides range from 0.0000467 to 0.0194 m^2 (Table 3).

Table 1- Volume calculations for the CRLC. The maximum value column is Surface Area multiplied by field-measured depths (found in Appendix B). Caluclated Volume column uses Eq. 1 derived from Guzzeti et al., 2008.

Landslide no.	Maximum Value (km^3)	Calculated Volume (km^3) (Guzzetti et al., 2009)
CRLC 28	4.29E-04	1.32E-02
CRLC 30	1.59E-03	1.94E-02
CRLC 32		4.67E-05
CRLC 33		7.43E-03
CRLC 27		1.05E-02
CRLC 26		2.37E-03
CRLC 25		6.16E-03
CRLC 22	1.54E-04	1.13E-03
CRLC 23		9.52E-04
CRLC 21		8.43E-03
Oso (Iverson et al., 2015)		8.30E-03

4.4 Landslide Mobility Indices

Generally, L/H values should increase as volume increases (Legros, 2002). The L/H of the CRLC ranges from 1.93 to 5.97 (Table 4). The CRLC falls into the normal range of mobility for

debris flows and flowslides (Fig. 9a). L/H values increase as landslide volume increases (Iverson et al., 2015).

The relationship between area and volume can loosely serve as a proxy for area affected by given debris flow (Iverson et al., 2015). Griswold and Iverson (2008) introduce a power-law relationship between *A* as a function of *V* (Fig. 9b). The $A/V^{2/3}$ coefficients of the CRLC range from 11 to 15 (Table 4), about half of the value for the Oso debris avalanche-flow (DAF; Iverson et al 2015).

Another index was necessary because L/H ratios can underrepresent mass flows saturated with water (Griswold and Iverson, 2008). Values for seismic velocity were collected by Landau Associates (2006). The density (ρ) of each flowslide is derived from the seismic velocity of Unit 1 and Eq. 4, which was found to be 247 kg/m^3 (see Appendix D). Adding these data points to a semi-log graph of *A* as a function of ρgVH shows that all the CRLC plot below the power-log trend for other large high-mobility debris flows (Iverson et al., 2015; Fig. 9c).

Table 2- Summary of results of three different mobility indices.

Landslide no.	Calculated Volume (km^3)	L/H	$(A/V)^{2/3}$	ρgVH
CRLC 28	1.32E-02	4.49	11.14	8.03E+11
CRLC 30	1.94E-02	5.07	10.28	1.41E+12
CRLC 32	4.67E-05	3.80	35.80	5.41E+07
CRLC 33	7.43E-03	2.72	12.54	3.47E+11
CRLC 27	1.05E-02	5.46	11.66	5.11E+11
CRLC 26	2.37E-03	1.86	15.89	5.43E+10
CRLC 25	6.16E-03	3.71	13.04	2.20E+11
CRLC 22	1.13E-03	5.97	18.52	9.48E+09
CRLC 23	9.52E-04	1.93	19.18	1.09E+10
CRLC 21	8.43E-03	4.56	12.22	3.86E+11
Oso (Iverson et al., 2015)	8.30E-03	10.53	27.55	2.80E+13

4.5 Landslide Age Analysis

4.5.1 Absolute Ages

Three charcoal samples were dated from soils underlying two flowslides in the CRLC (Fig. 4). Radiocarbon dates from beneath CRLC 30 range from 1731 to 1891 calendar ^{14}C Yr B.P. The soil underlying CRLC 22 had one radiocarbon date of 4527 calendar ^{14}C B.P. Volcanic ash from the same soil is a mix of 90% Mazama Climactic Tephra (6850 14C BP and 10% Glacier Peak Dusty Creek tephra [5780-5830 ^{14}C BP]). A date from the soil below CRLC 28 is 170 ^{14}C Yr B.P. (Table 5).

Table 3- Results from Radiocarbon dating of wood and charcoal material found in Cedar River Watershed. For sample locations, see Fig. 4. Data processed by DirectAMS in Bothell, WA, Beta Analytics in Miami, FL and the GeoAnalytical Lab at Washington State University in Pullman, WA.

Sample #	Sample Material	Deposit	Average SDS value (°)	Radiocarbon Age (1σ error)	Yr Cal BP (1σ error)
10B	Charcoal	CRLC 30	3.26	1891 ±34	1857-1925
10C	Charcoal	CRLC 30	3.26	1731±30	1701-1761
8C	Charcoal	CRLC 22	3.35	4527 ±56	4471-4583
	Volcanic Ash	CRLC 22	3.35	6850	5780-6850
7A	Bark	CRLC 28	3.32	170±30	140-200

4.5.2 Surface Roughness

Using the roughness measure of standard deviation of slope (SDS), an average value for each flowslide was calculated. SDS values for the main bodies of the CRLC ranged from 3.06° to 3.35°. In the additional calculation considering only the toe and lateral levees of the slide deposits, the average SDS values range from 4.15° to 4.43°.

The calibrated roughness-age curve from the North Fork Stillaguamish River Valley (LaHusen et al., 2016) does not sufficiently predict the age of the CRLC landforms. This model over estimates the calibrated dates by several thousand years (Table 6; Fig. 10).

Table 4- Surface roughness values for CRLC units. Whole slide body average SDS values to the left and toe and lateral levee only values to the right. The table is sorted by toe SDS values because there is a weak correlation between the toe SDS value and the absolute ages.

Landslide no.	Average SDS value (°) *Whole Slide*	Average SDS value (°) *Toe/Levee Only*	Calibrated Yr BP	Estimated Yr BP (LaHusen et al., 2016)
26	3.33	--		--
27	3.28	**4.15**		8785
23	3.26	**4.17**		8660
33	3.06	**4.19**		8540
30	3.26	**4.26**	1731-1891	8130
25	3.35	**4.28**		8015
32	3.3	**4.33**		7740
21	3.35	**4.33**		7740
22	3.35	**4.43**	4527-6850	7210
28	3.32	**4.51**	170	6815

5.0 Discussion

5.1 Flowslide Morphologies

Using established mobility indices allows us to place the CRLC in a regional and worldwide context (Iverson et al 2015). Most of the larger members of the CRLC show similar morphology (Fig. 4). The L/H ratios for the CRLC range from about one third to about half of the 2014 Oso event, but the Oso event had three times the volume (Fig. 9a). The $A/V^{2/3}$ coefficients of the CRLC weakly follow the power relationship between *A* and *V* (Fig. 9b), suggesting the CRLC impacted about the same amount of area as other large debris flows (Iverson et al., 2015). The CRLC falls well below worldwide averages for R_s, suggesting the CRLC events had very little potential energy (Iverson et al., 2015). Therefore, the CRLC has average runout, affected an average area, and had less than average energy.

To be classified a debris flowslides, a mass wasting event is driven by liquefaction and excessive pore pressures. If rotated blocks are present, the CRLC would not be a series of flowslides, instead they would be classified as rotational slide-earthflows (Hungr et al., 2014).

All landslides in the CRLC show a distinct feature near the crown, a topographic bench near their head scarps (Fig. 6). This bench is approximately the same elevation (300m) across each landslide and speculated by some workers to be rotated blocks (Stoker, per comm., 2016). GPR was collected along the bench to determine if the bench is depositional or rotational. If the bench is intact Unit 3, bedding should be near horizontal. Radargrams of the survey results show no rotated units (Fig. 8), suggesting the feature is a depositional bench (Jacobacci, per comm., 2017), which supports the cross section created by Landau Associates (2006; Fig. 11). Unit 3 bench could have been unroofed during the landsliding process, but is not landslide material.

Although the Oso landslide and CRLC slides both occurred in glacial material (Riemer et al., 2015), the stratigraphy at the two sites is quite different. The CRLC occurred in a terminal moraine of gravels and sands (Mackin, 1941), whereas Oso occurred in a typical glacial advance sequence, including gravels, sands and lacustrine clays and silts (Riemer et al., 2015; LaHusen et al., 2016). Therefore, the Oso deposits contain a wide range of grain sizes, including fines. The CRLC units have no source of fine material, and are coarser than the Oso deposits (Fig. 11). There is a lacustrine unit present up-valley in the Cedar River (Mackin, 1941; Landau Associates, 2006), but it was not observed at this site.

Previous work in the Cedar River has focused on permeability and seepage problems at the Chester Morse dam (Mackin, 1941; Landau Associates, 2006). At Hobo Springs, just downhill from the Masonry dam (Fig. 2), a very detailed cross section has been created, including two Vashon glacial units and an older, consolidated unit (Fig. 11). Unit 1L is interpreted as Unit 1 from the Landau Associates report because it is weakly stratified, loose density (Table 1) and contains green metamorphosed lithics (Appendix C). This unit is a recessional outwash and can have a veneer of till (Mackin, 1941; Landau Associates, 2006), but till was not observed at Site 1. Unit 5L is very dense and corresponds to Unit 3 (Landau Associates, 2006; Galster and Laprade, 1991). Up-valley, Unit 3 forms a bench-like feature

beneath Unit 1 and 2 (Fig. 11). The bench, composed of older, pre-Frasier glacial Unit 3, is overridden and very dense (Landau Associates, 2006).

5.2 Surface Roughness and Age Correlations

SDS does not appear to work as a good proxy for landslide age in the CRLC. SDS values for the whole slide and toe/levee do not show a correlation with age (Fig. 13). Landforms 23 and 33, which are interpreted as remobilizations of landforms 21 and 30 respectively, have lower average values than the original landform. In the field, cross cutting relations determined that landform 21 is older than landform 22 (10.6 Appendix B), this is not reflected in the surface roughness values (Table 6).

The average surface roughness values for the CRLC have a large spread in age and yet a very small range in average SDS values (Table 6). Previous authors found a correlation between median roughness and age, rougher landforms are younger (Frankel and Dolan, 2007; Goetz et al., 2014; LaHusen et al., 2016; Booth et al., *in press*). At the CRLC, no correlation was found in the data (Fig. 13).

The relationship between surface roughness and landslide age is still debated. Using a similar methodology to this study, Goetz et al. used an inventory of 12 flowslides and short time scales to determine ages of mass wasting. The authors found surface roughness to be a poor proxy for landslide age, suggesting with such a small inventory that lithology and reactivation of landslides could affect the relationship (Goetz et al., 2014). The results of this study might be limited by the inventory size and similar time scales. Other authors have found stronger relationships when using large subsets of events with similar failures occurring over long time scales and in similar substrates (LaHusen et al., 2016; Booth et al., *in press*).

This small of range in values and the wide range in ages suggests either a simple diffusion creep law is not appropriate at this site, a much smoother initial roughness than expected, or that the radiocarbon ages (which are not on the actual landslide itself, but a soil below and thus only place limits on the maximum landslide age) are not tightly bracketing the slide age.

Additional considerations relate to human interference with the landscape. Accounting for the potential smoothing caused by coal mining in the region, the average roughness of each CRLC unit could be further decreased by 0.5° (Pollock, 2015). The Cedar River area has more anthropogenic disturbances over longer periods of time. If the land were flattened or graded by logging activities, average SDS values would be smaller. Surface roughness should decrease with time due to surface erosion, weathering and vegetation (Glenn et al., 2006), and the correlation between age and surface roughness appears to weaken with older slides (Goetz et al., 2014).

The weak correlation between age and roughness could suggest different dominant diffusion processes at Cedar River than NFSR, possibly caused by dense vegetation or coarser material. The model created for NFSR tracks the diffusion of the landscape through time (LaHusen et al., 2016; Booth et al., *in press*). As such, it is dependent upon the diffusivity (K) of the hillslope. The transport law of soils can be written

$$-\frac{\partial x}{\partial t} = \frac{1}{\rho_b}\frac{\partial}{\partial x}\left(-K\frac{\partial z}{\partial z}\right) \quad (4)$$

where *z* is elevation, *x* is distance from watershed divide and ρ_b is soil density. If *K* is constant along a hillslope profile (an accurate assumption in the Cedar River with 200m of relief), a diffusion coefficient *D* (with units L^2/T) can be written

$$\frac{\partial z}{\partial t} = D\frac{\partial^2 t}{\partial x^2} \quad (5)$$

where *t* is time. Therefore, *D* can be set equal to K/ρ_b (Fernandes and Dietrich, 1997). With coarser grained material, less density is expected at Cedar River as fewer fine particles are present to fill in the void space between larger sediments. The high permeability of the gravels (Mackin, 1941) will also increase *D*. The expected result is a higher value of *D* at the Cedar River and more diffusion through time. With a higher value for *D*, it can be expected that the features of the CRLC would be more diffuse at younger ages.

Dating organics found at the base of a landslide provides a maximum age for the movement (Lang et al., 1999) and since 2000 has been used in 11% of landslide dating surveys (Pánek, 2015). This method is considered the most reliable when dating debris flows (Lang et al., 1999). In this study, dateable wood was collected from the base of landslide material in soil horizons. The position of the wood indicates placement a short time before the movement of the slide (Stout, 1969). The soil horizons appeared fresh and no evidence of scour was observed in the field in all but one pit (slickensides observed at the flowslide base, 10.3 Appendix B), so the observed soil horizons are assumed to be the paleosurface at the time of the flowslides. However, it is possible this surface was exposed for hundreds to thousands of years before the landslide.

5.3 Landslide Triggers

During and just after glacial retreat conditions at the terminal moraine would have been ideal for slope failure, i.e. saturated and oversteepened (Booth, 1986). The flowslides could possibly have been triggered as the glacial meltwater flowed through the permeable embankment. Such conditions have triggered debris flows originating from highly permeable morainal slopes for hundreds of years after glacial retreat (Palacios et al., 1999; O'Connor et al., 2001; Holm and Jakob, 2004). However, with a wide range of ages much younger than the time of glacier retreat, it seems unlikely these features formed as relict glacial age features.

If the CRLC were triggered by a single seismic event, we would expect a tight grouping of ages. We instead see a wide spread in ages. In addition, none of the absolute ages in the Cedar River overlap with the timing of known seismic events in the region or with the spike in landslides Booth et al. (*in press*) observed at 900-1300 Yr B.P. and 500 to 700 Yr B.P., possibly related to earthquake activity.

Precipitation is a major factor of unstable slopes in the region (Chleborad, 2000). As such, we cannot rule it out as a potential trigger for the CRLC failures. Landslides in Seattle can be triggered by high-intensity storm events with as little as 1 inch of precipitation in the preceding 3 days (Chleborad, 2000). Due to lack of pre-historic precipitation data, we must assume that

precipitation-triggered landslides could happen at any time and any date. Without precipitation data, a precipitation trigger can never be fully ruled out.

6.0 Concluding Remarks

Previous failures in the Cedar River valley and the recently discovered CRLC highlight the hazards associated with coarse grained glacial material. The eight flowslides of the CRLC exhibit normal to low mobility (Fig. 9), but have a wider range in ages than the range in average SDS values suggest (Table 6). The model created for the NFSR (LaHusen et al., 2016) could not be used for dating the CRLC in the Cedar River Municipal Watershed.

Future work at the CRLC could focus on calibrating a surface roughness to age curve. This would require more absolute dates for each flowslide, probably through more organic samples to be radiocarbon dated.

7.0 References

Arguez, A., Durre, I., Applequist, S., Vose, R.S., Squires, M.F., Yin, X., Heim, R.R., Owen, T.W., 2012, NOAA's 1981-2010 U.S. Climate Normals: an overview. Bull. Am. Meteorological Soc. 93 (11), 1687e1697. http://dx.doi.org/10.1175/bams-d- 11-00197.1.

Bell, R., Petschko, H., Roehrs, M., and Dix, A., 2012, Assessment of landslide age, landslide persistence and human impact using airborne laser scanning digital terrain models: Geografiska Annaler, ser. A, v. 94, p. 135–156, doi:10.1111/j.1468-0459.2012.00454.x.

Berti, M., Corsini, A., and Daehne, A., 2013, Comparative analysis of surface roughness algorithms for the identification of active landslides: Geomorphology, v. 182, p. 1–18, doi:10.1016/j.geomorph .2012 .10.022.

Booth, A.M., LaHusen, S.R., Duvall, A.R., and Montgomery, D.R., 2016, Holocene history of deep-seated landsliding in the North Fork Stillaguamish 1 River valley from surface roughness analysis, radiocarbon dating, and 2 numerical landscape evolution modeling: (in press).

Booth, D. B., 1986, The formation of ice-marginal embankments into ice-dammed lakes in the eastern Puget Lowland, Washington, USA, during the late Pleistocene: Boreas, v. 15(3), p. 247-263.

Cedar River Municipal Watershed, 2012, Historic Taylor: Seattle, Seattle Public Utilities, 11 p.

Cedar River Municipal Watershed, 2013, Railroad History: Seattle, Seattle Public Utilities, 11 p.

Chleborad, A.F., 2000, Preliminary method for anticipating the occurrence of precipitation-induced landslides in Seattle, Washington: U.S. Geological Survey Open-File Report 2000-469, 29 p., http://pubs.usgs.gov/of/2000/0469/report.pdf.

City of Seattle, 2000, Cedar River Watershed Habitat Conservation Plan for the Issuance of a Permit to Allow Incidental Take of Threatened and Endangered Species:

Dade, W.B. and Huppert, H.E., 1998, Long-runout rockfalls: Geology v. 26, p. 803–806.

Dragovich, J. D.; Walsh, T. J.; Anderson, M. L.; Hartog, Renate; DuFrane, S. A.; Vervoot, Jeff; Williams, S. A.; Cakir, Recep; Stanton, K. D.;Wolff, F. E.; Norman, D. K.; Czajkowski, J. L., 2009, Geologic map of the North Bend 7.5-minute quadrangle, King County, Washington, with a discussion of major faults, folds, and basins in the map area: Washington Division of Geology and Earth Resources Geologic Map GM-73, 1 sheet, scale 1:24,000, with 39 p. text.

Fernandes, N. F., and Dietrich, W. E., 1997, Hillslope evolution by diffusive processes: The timescale for equilibrium adjustments: Water Resources Research, v. 33(6), p. 1307-1318.

Frankel, K.L., and Dolan, J.F., 2007, Characterizing arid region alluvial fan surface roughness with airborne laser swath mapping digital topographic data: Journal of Geophysical Research, v. 112, p. F02025.

Frizzell, Y. A. Jr. Tabor. R. W., Booth, D. B. and Waitt, R. B. Jr., 1984, Preliminary geologic map of the Snoqualmie 1: 100,000 quadrangle. Washington: U. S. Geological Survey Open-File Report 84493.

Galster, R. W. and Laprade, W. T., 1991, Geology of Seattle, Washington, United States of America: Environmental & Engineering Geoscience, v. 28(3), p. 235-302.

Glenn, N. F., Streutker, D. R., Chadwick, D. J., Thackray, G. D., and Dorsch, S. J., 2006, Analysis of LiDAR-derived topographic information for characterizing and differentiating landslide morphology and activity: Geomorphology, v. 73(1), p. 131-148.

Goetz, J. N., R. Bell, and A. Brenning, 2014, Could surface roughness be a poor proxy for landslide age? Results from the Swabian Alb, Germany: Earth Surface Processes and Landforms, v. 39, p. 1697-1704, doi:10.1002/esp.3630.

Griswold, J.P., Iverson, R.M., 2008. Mobility statistics and automated hazard mapping for debris flows and rock avalanches. U.S. Geol. Surv. Sci. Invest. Rep. 2007-5276, 59 p. http://pubs.usgs.gov/sir/2007/5276/.

Grohmann, C.H., Smith, M.J., and Riccomini, C., 2011, Multiscale analysis of topographic surface roughness in the Midland Valley, Scotland: IEEE Transactions on Geoscience and Remote Sensing, vol. 49(4), p. 1200-1213.

Guzzetti, F., Ardizzone, F., Cardinali, M., Rossi, M., and Valigi, D., 2009, Landslide volumes and landslide mobilization rates in Umbria, central Italy: Earth and Planetary Science Letters, v. 279(3), p. 222-229.

Guzzetti, F., Mondini, A.C., Cardinali, M., Fiorucci, F., Santangelo, M., and Chang, K.T., 2012, Landslide inventory maps: New tools for an old problem: Earth-Science Reviews, vol. 112(1-2), p. 42-66.

Henn, B., Cao, Q., Lettenmaier, D.P., Magirl, C.S., Mass, C., Bower, J.B., St. Laurent, M., Mao, Y., Perica, S., 2015. Hydroclimatic conditions preceding theMarch 2014 Oso landslide. J. Hydrometeorol. 16, 1243–1249. http://dx.doi.org/10.1175/JHM-D-15-0008.1.

Holm, K., Bovis, M., and Jakob, M., 2004, The landslide response of alpine basins to post-Little Ice Age glacial thinning and retreat in southwestern British Columbia: Geomorphology, v. 57(3), p. 201-216.

Hovius, N., Stark, C. P., and Allen, P. A., 1997, Sediment flux from a mountain belt derived by landslide mapping: Geology, v. 25(3), p. 231-234.

Hsu, K., 1978. Albert Heim: observations on landslides and relevance to modern interpretations. In: Voight, B. (Ed.), Rockslides and Avalanches. In: Natural Phenomena, vol.1. Elsevier, Amsterdam, p.71-93.

Hungr, O., 2007, Dynamics of rapid landslides. *In* Fukuoka, H., ed., Progress in Landslide Science, Springer Berlin Heidelberg, p. 47-57.

Hungr, O., Leroueil, S., and Picarelli, L., 2014, The Varnes classification of landslide types, an update: Landslides, v. 11(2), p. 167-194.

Iverson, R.M., George, D.L., Allstadt, K., Reid, M.E., Collins, B.D., Vallance, J.W., Schilling, S. P, Godt, J.W., Cannon, C.M., Magirl, C.S., Baum, R.L., Coe, J.A., Schulz, W.H., Bower, J. B, 2015, Landslide mobility and hazards: Implications of the 2014 Oso disaster: Earth and Planetary Science Letters, v. 412, p. 197–208, doi:10.1016/ j.epsl.2014.12.020.

Keaton, J.K., Wartman, J., Anderson, S., Beno.t, J., deLaChapelle, J., Gilbert, R., and Montgomery, D.R., 2014, The 22 March 2014 Oso Landslide, Snohomish County, Washington: Geotechnical Extreme Events Reconnaissance Association ReportGEER-036, 186 p., http:// snohomishcountywa.gov /DocumentCenter /View /18180.

Kottek et al., (2006), World map of Köppen-Geiger climate classification updated: Meteorology Zeitschrift, v. 15, p. 259-263, http://koeppen-geiger.vu-wein.ac.at.

LaHusen, S.R., Duvall, A.R., Booth, A.M., Montgomery, D.R., 2016, Surface roughness dating of long-runout landslides near Oso, Washington (USA), reveals persistent postglacial hillslope instability: Geology, v. 44.2, p.111-114.

Landau Associates, 2006, Cedar moraine safety studies final report—Cedar River watershed, King County, Washington: Landau Associates, 1 v., 1 DVD.

Lang, A., Moya, J., Corominas, J., Schrott, L., and Dikau, R., 1999, Classic and new dating methods for assessing the temporal occurrence of mass movements: Geomorphology, v. 30, p. 33–52.

Larsen, I. J., Montgomery, D. R., and Korup, O., 2010, Landslide erosion controlled by hillslope material: Nature Geoscience, v. 3(4), p. 247-251.

Legros, F., 2002, The mobility of long-runout landslides: Engineering Geology, v. 63, p. 301-331.

Mann, A. G., Tam, C. C., Higgins, C. D., and Rodrigues, L. C., 2007, The association between drinking water turbidity and gastrointestinal illness: a systematic review: BMC Public Health, vol. 7(1), p. 256.

Mackin, J. H., 1941a, A geologic interpretation of the failure of the Cedar Reservoir, Washington: University of Washington Engineering Experiment Station Bulletin, v. 107, p. 30.

O'Connor, J. E., Hardison, J. H., & Costa, J. E., 2001, Debris flows from failures of Neoglacial-Age moraine dams in the Three Sisters and Mount Jefferson wilderness areas, Oregon: U.S. Geological Survey Open-File Report 2001-1606, 105 p., https://pubs.usgs.gov/pp/1606/report.pdf.

Palacios, D., Parrilla, G., and Zamorano, J.J., 1999, Paraglacial and postglacial debris flows on a Little Ice Age terminal moraine: Jamapa Glacier, Pico de Orizaba (Mexico): Geomorphology, v. 28(1), p. 95-118.

Pánek, T., 2015, Recent progress in landslide dating: A global overview: Progress in Physical Geography, v. 39(2), p. 168-198.

Pollock, M.J., 2015, Geomorphic Differences between Unmined and Surface Mined Lands in Southeastern Ohio [Ph.D. Thesis] Ohio State University, 141 p.

Porter, S.C., and Swanson, T.W., 1998, Radiocarbon age constraints on rates of advance and retreat of the Puget lobe of the Cordilleran ice sheet during the last glaciation: Quaternary Research, v. 50, p. 205–213, doi:10.1006/qres.1998.2004.

PSLC. 2014. Puget Sound Lidar Consortium. Cedar River Watershed & Floodplain, Lake Youngs Reservoir, & SCL/Tolt Reservoir Study Areas LiDAR, Technical Data Report – Delivery 2, revised October 22, 2014. Flown on October 29 – 30, 2013, November 1, 3 - 4, 2013, December 3 – 5, 2013, February 5 – 7, 2014, June 22, 23, 30, 2014, and July 2, 5 - 8, 2014. Projection: Washington State Plane North Horizontal Datum: NAD83 (HARN*) Vertical Datum: NAVD88 (GEOID03) Units: US Survey Feet. http://pugetsoundlidar.ess.washington.edu/lidardata/proj_reports/Cedar_Watershed_LiDAR_Report_Delivery_2_Revised.pdf

Riemer, M.F., Collins, B.D., Badger, T.C., Toth, C., and Yat Chun, Y., 2015, Geotechnical soil characterization of intact Quaternary deposits forming the March 22, 2014 SR-530 (Oso) landslide, Snohomish County, Washington: U.S. Geological Survey Open-File Report 2015-1089, 17 p., http://dx.doi.org/10.3133/ofr20151089.

Seattle Municipal Archives, 2010, Seattle City Archives, accessed March 2017 from <http://www.seattle.gov/cityarchives>.

Seattle Public Utilities, 2016, Cedar River Municipal Watershed (Lower Portion), City of Seattle, accessed July 2016 from <http://www.seattle.gov/util/cs/groups/public/@spu/@conservation/documents/webcontent/spu01_003240.pdf>.

Stoker, B. 2016, Cedar Watershed Landslide and Active Landform Mapping, Earth Systems, v. 3.5.

Stout, M., 1969, Radiocarbon dating of landslides in southern California and engineering geology implications: Geological Society of America Special Paper 123, p. 12 p.

Thorson. R. M. l9lll: Isostatic effects of the last glaciation in the Puget lowland. Washington. U.S: U.S. Geological Survey Open-File Report 81-370. LX. l pp.

Varnes, D. J., 1978, Slope movement types and processes, in Schuster, R. L., and Krizek, R. J., eds., Landslides analysis and control: Washington, D.C., National Research Council, Transportation Research Board Special Report 176, p. 11–33.

Wang, G., and Sassa, K., 2003, Pore-pressure generation and movement of rainfall-induced landslides: Effects of grain size and fine-particle content: Engineering Geology, v. 69(1), p. 109-125.

Wartman, J., Montgomery, D. R., Anderson, S. A., Keaton, J. R., Benoît, J., de la Chapelle, J., and Gilbert, R., 2016, The 22 March 2014 Oso landslide, Washington, USA: Geomorphology, v. 253, p. 275-288.

Wen, B. P., Aydin, A., Duzgoren-Aydin, N. S., Li, Y. R., Chen, H. Y., and Xiao, S. D., 2007, Residual strength of slip zones of large landslides in the Three Gorges area, China: Engineering Geology, v. 93(3), p. 82-98.

8.0 Figures

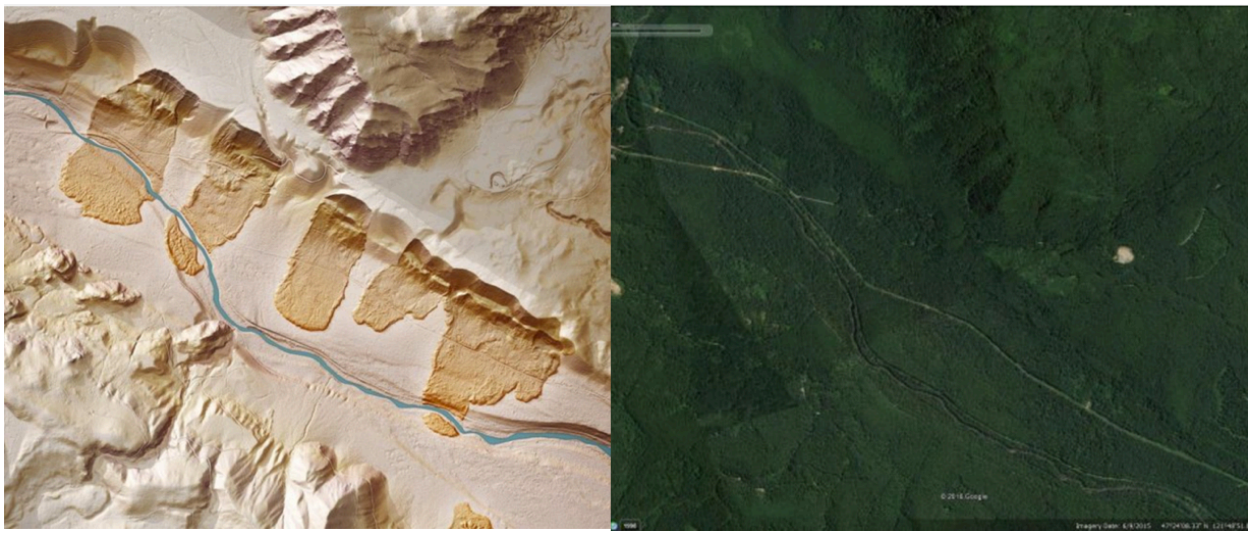

Figure 1- Comparing LiDAR image (left) to aerial photo (right) or the CRLC. The debris flows are not visible on aerial photography and therefore not discovered until LiDAR became available.

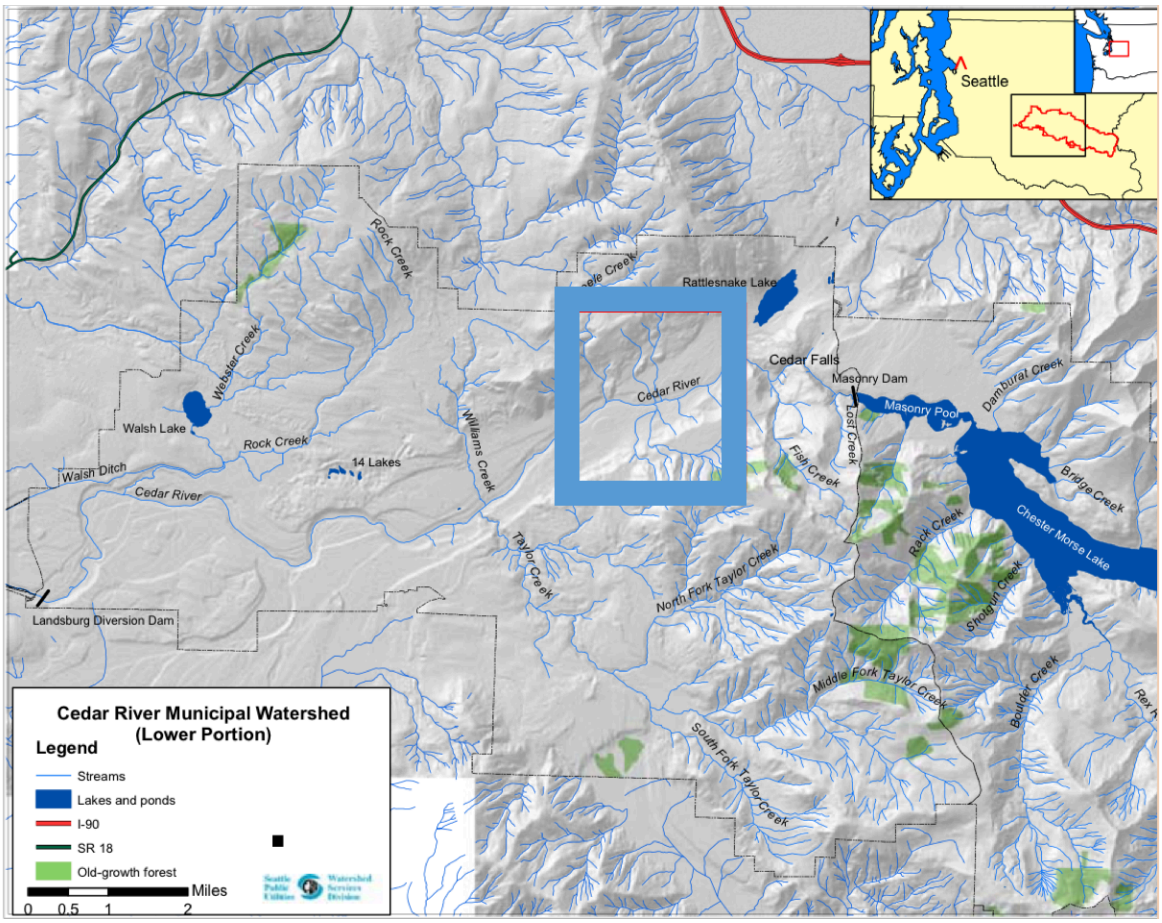

Figure 2- Regional geographic setting of study area (in blue square). Boundaries of Cedar River Municipal Watershed are in red

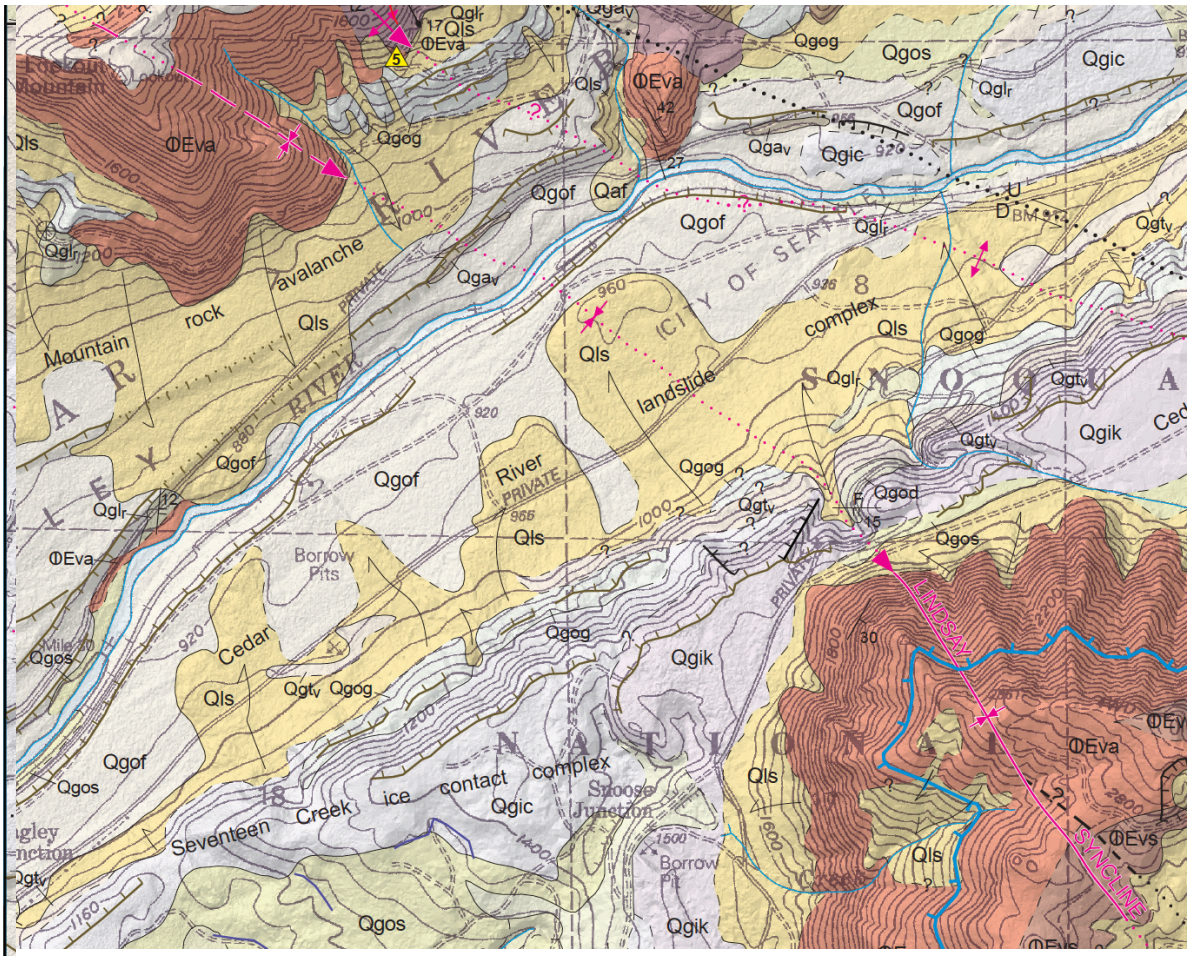

Figure 3- Section of geologic map of North Bend Quadrangle (from Dragovich et al., 2009). Includes the original mapping of the Cedar River Landslide Complex (CRLC) and the location of Seventeen Creek Ice contact complex (SCICC) just upslope. The Cedar kame terrace is upvalley from the SCICC in the right center of this image, but the label was cut off.

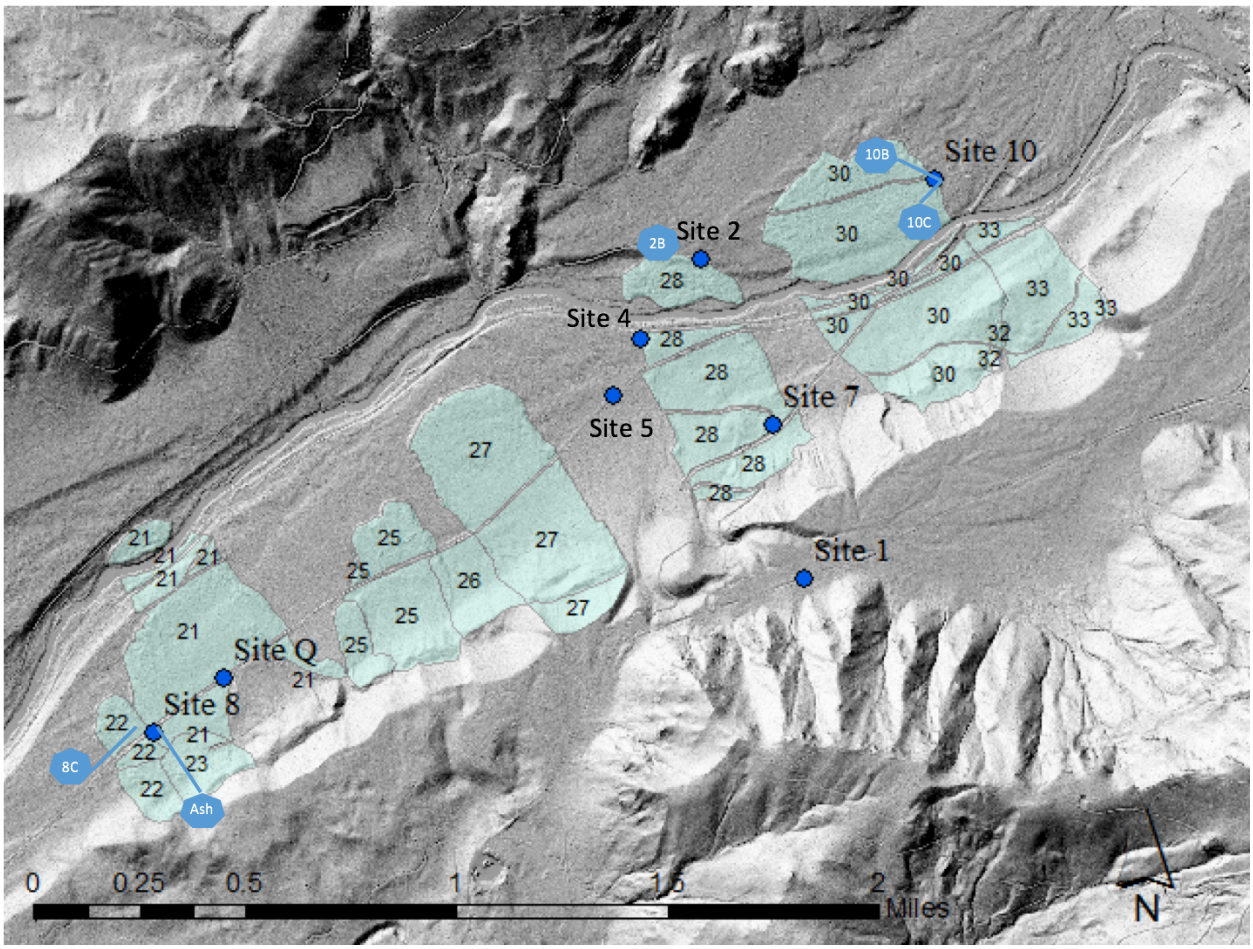

Figure 4- Cedar River Landslide Complex (CRLC) Cedar River Municipal Watershed. Blue polygons are units, labeled as in Stoker (2016). Red pins are field sites, including absolute dates found at each site. See Table 6 for dates

Figure 5- Town of Mocton, Washington inundated by floodwaters beginning in the spring of 1915. The site is now Rattlesnake Lake (Seattle Municipal Archives, 2010)

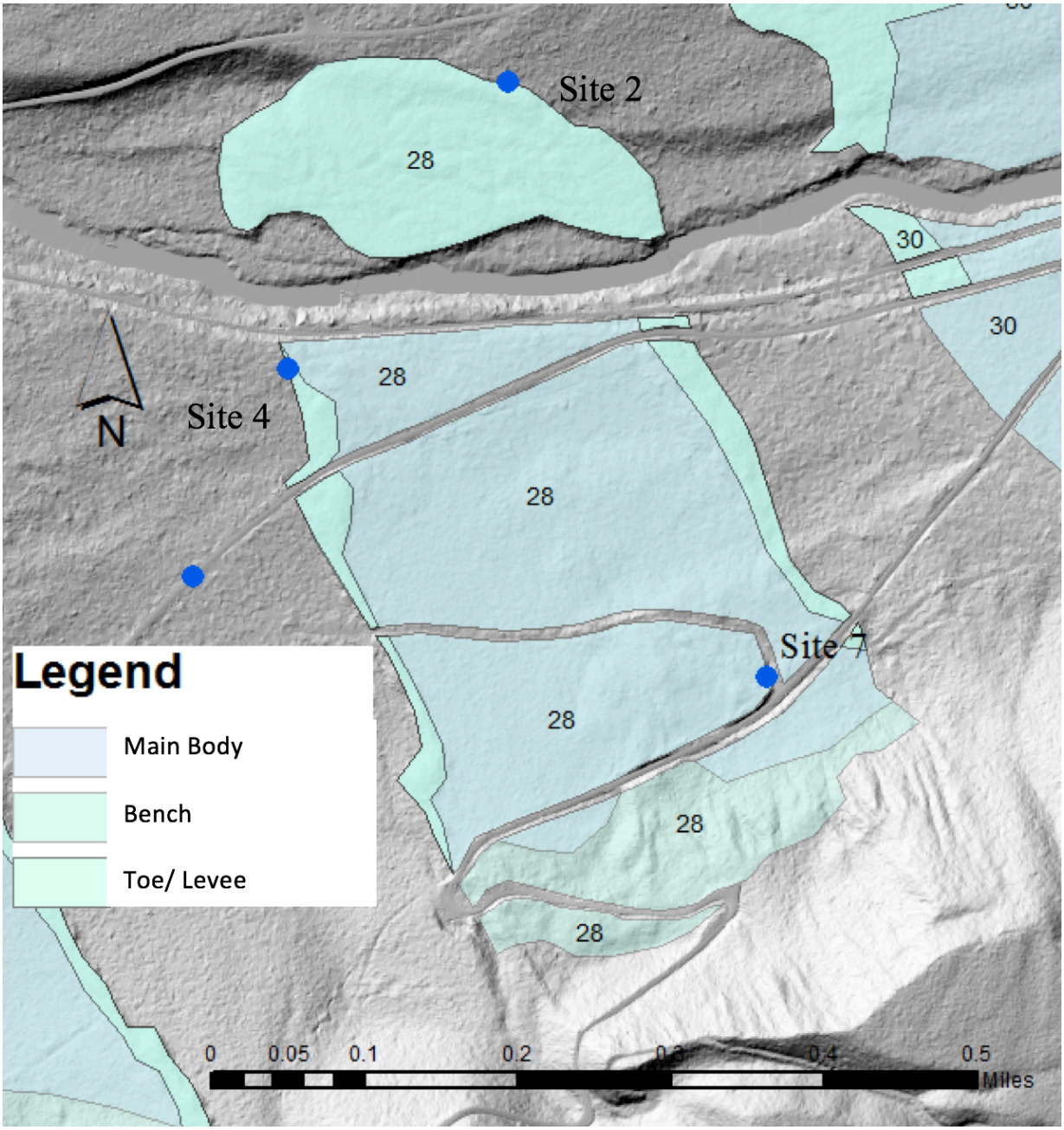

Figure 6- Landslide Zones. Main head scarp is located just up slope from the bench and just above the scale in this image. Three zones were identified in the CRLC, the depositional bench feature exposed near the scarp, the main body of the slide, and the toes and levee system along the margins

.

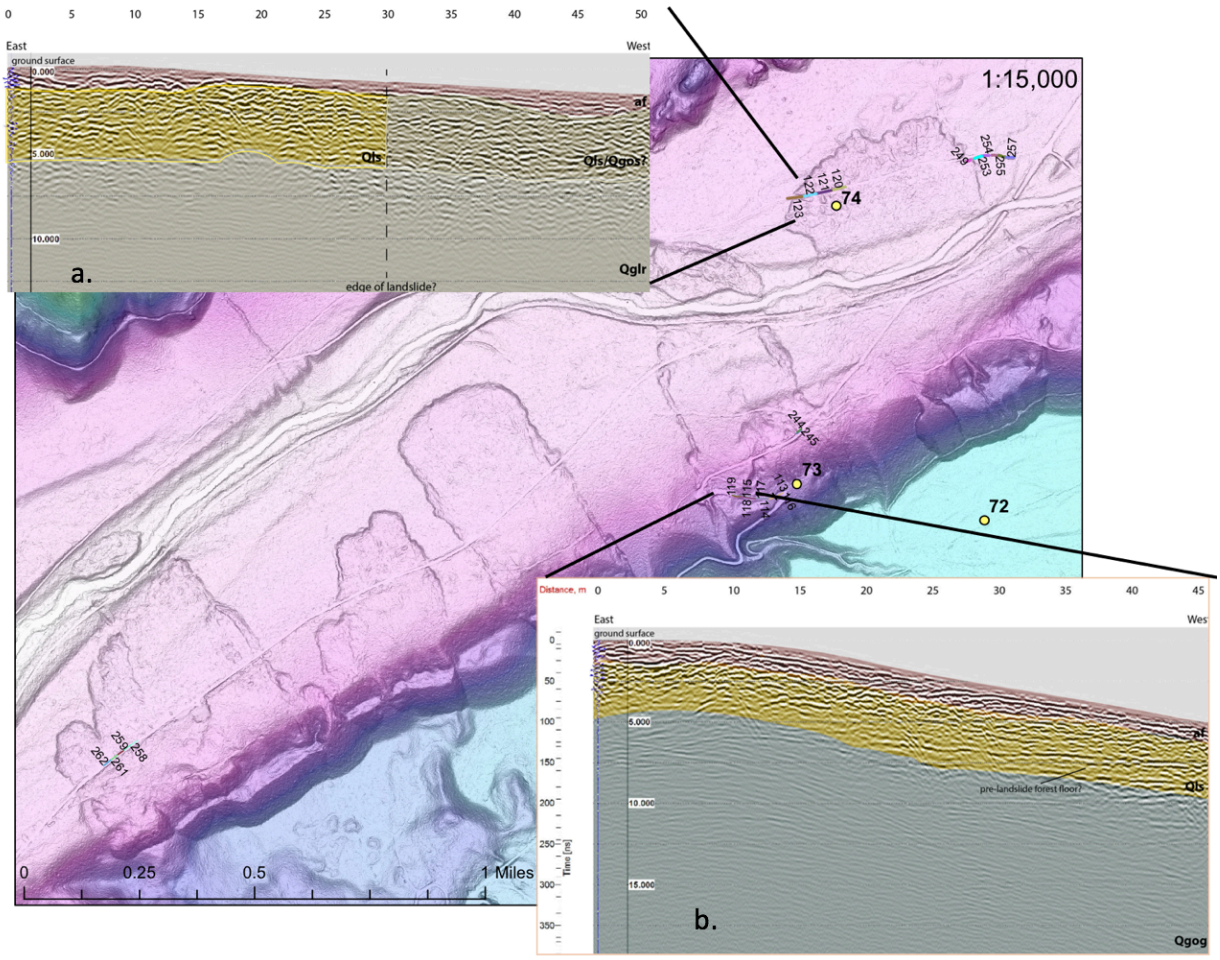

Figure 7- Ground Penetrating Radar (GPR) Survey results (from Jacobacci per comm., 2017). Underlying map includes survey locations. Yellow dots are passive seismic data collection sites, data unavailable at time of writing. Inserts are two examples of radargrams produced from results.

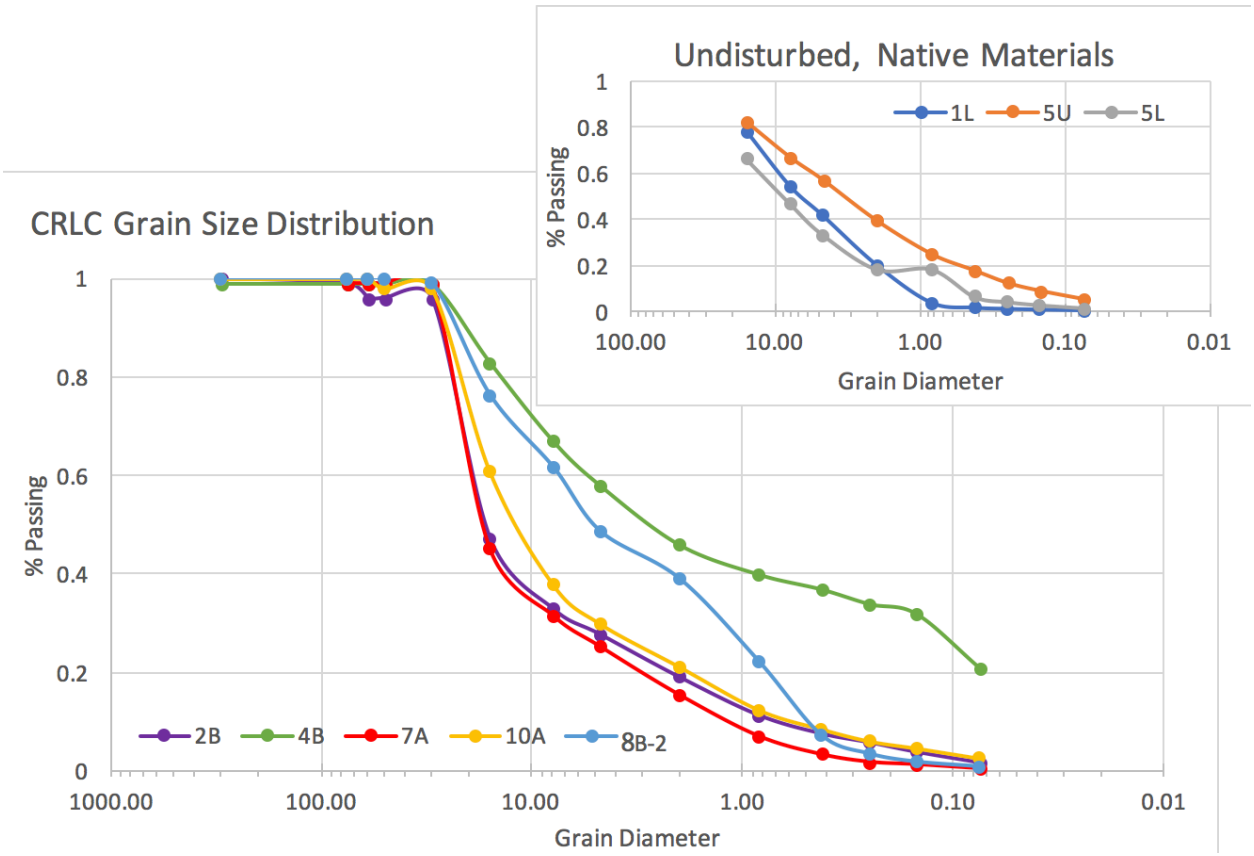

Figure 8- Grain Size Distributions of native, undisturbed material and CRLC units collected in the field. Sieve analysis results are compiled in Appendix A and site descriptions are compiled in Appendix B.

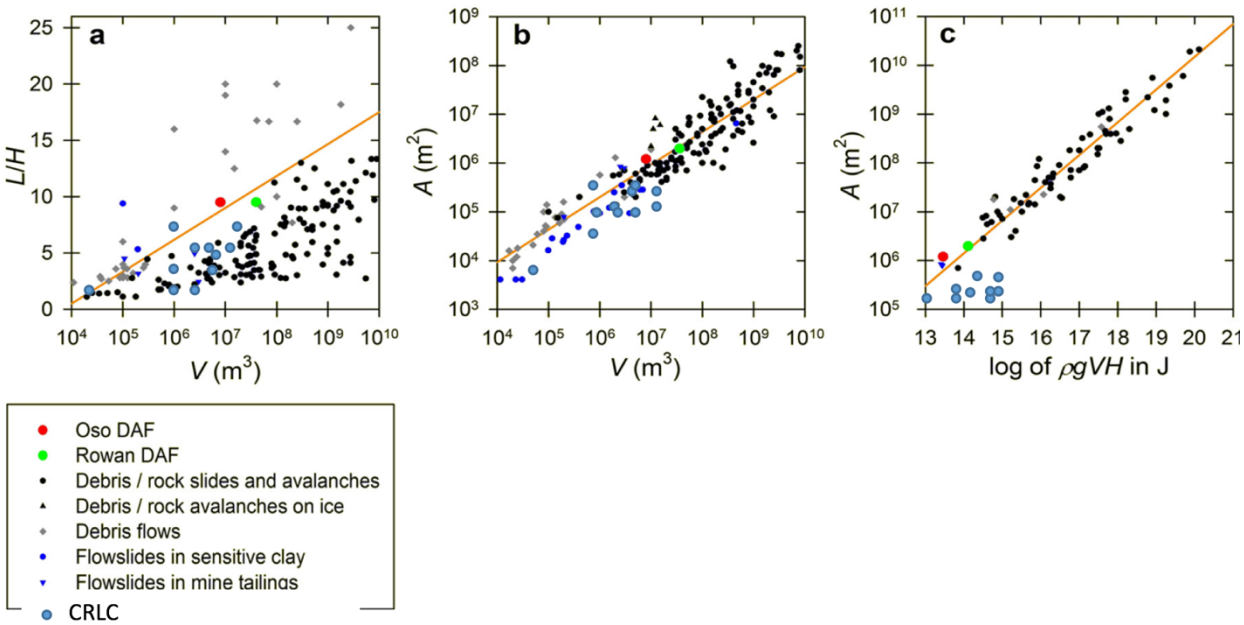

Figure 9- Mobility-index graphs for diverse high-speed landslides, including worldwide data from several sources as well as data for the Oso DAF and the Rowan DAF, a prehistoric landslide about 1 km west of the Oso DAF site. Each graph displays data for somewhat different sets of landslides, because few studies report all morphometric quantities needed to compile all three graphs. Orange line in panel c is the empirical power-law fit (Iverson et al., 2015).

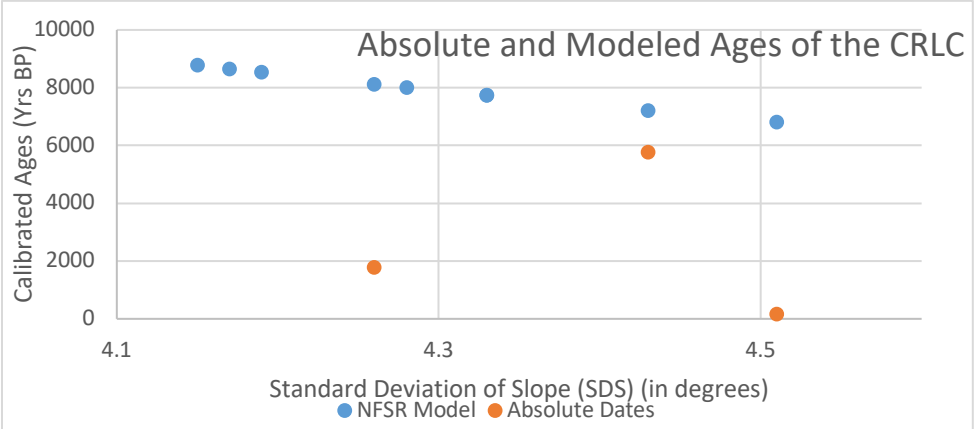

Figure 10- Ages of the CRLC from absolute dates (orange) and ages generated by the model of LaHusen et al. (2016). The modeled ages do not match the absolute ages and the absolute ages do not have a strong pattern.

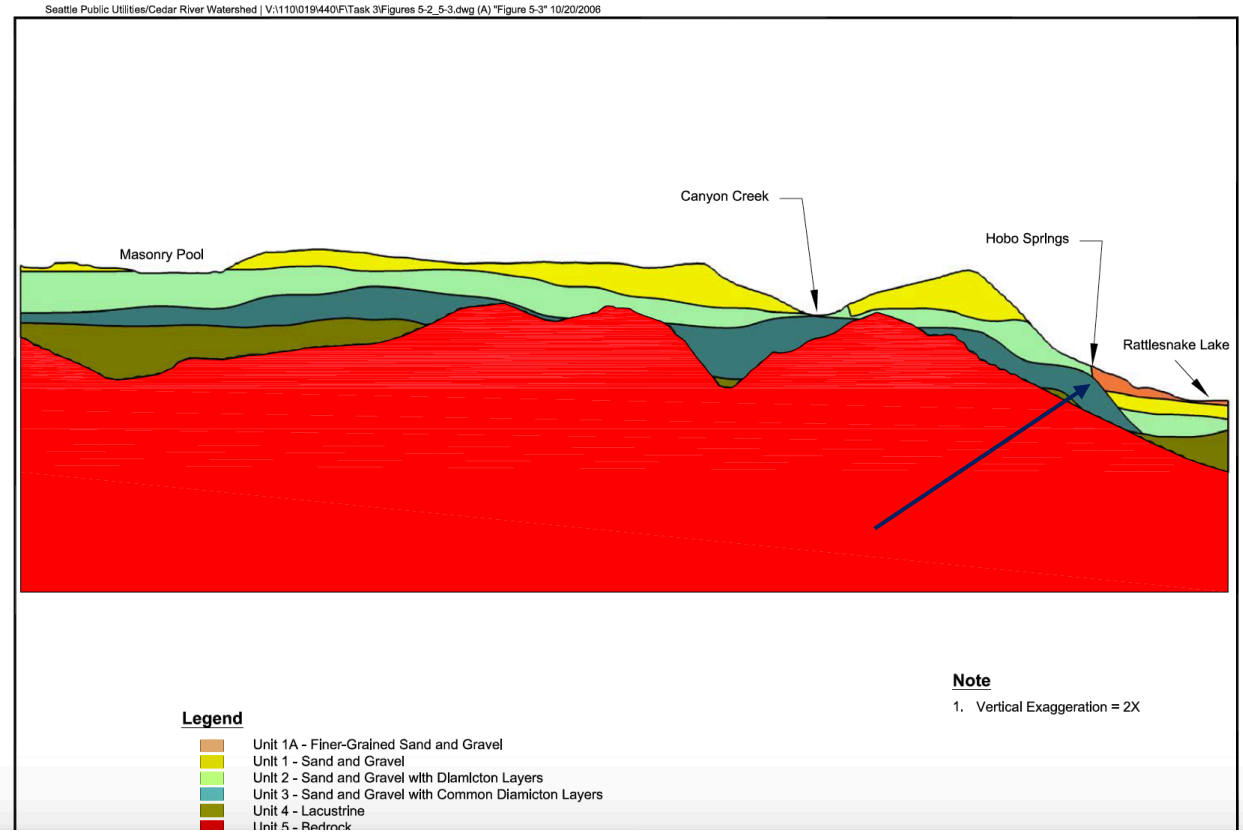

Figure 11- Cross section created by Landau Associates (2006). Cross section is located directly upslope from CRLC approximately three km (at "Masonry Dam" in Fig. 2). This report speculates the bench in Unit 3 just below the label for Hobo Springs possibly crops out at the CRLC. Arrow points to suspected bench feature.

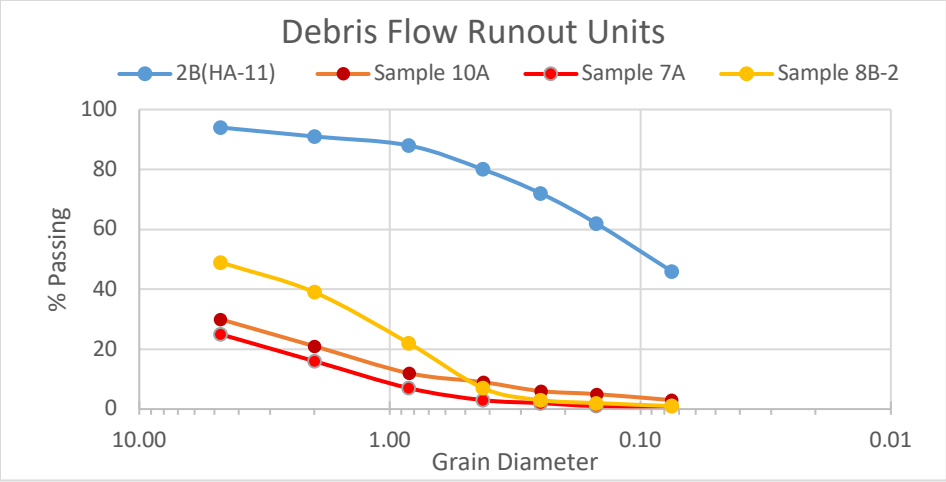

Figure 12- Comparison between Oso sample [2B(HA-11) data from Keaton et al., 2014] and CRLC samples. The sample from Oso are finer grained than the CRLC.

9.0 Appendix A

Sieve analysis results and photographs of dried and sieves samples

Site 1			
Sieve Size	Sieve Opening (mm)	1-M	1-L
"5/8 in"	15.875	75.1%	78.3%
"5/16 in"	7.9375	63.2%	54.5%
# 4	4.75	54.5%	41.9%
# 10	2	39.7%	20.2%
# 20	0.84	28.0%	4.0%
# 40	0.425	19.1%	1.8%
# 60	0.25	14.2%	1.3%
# 100	0.15	9.5%	1.0%
#200	0.075	5.1%	0.7%
	water content (w)	26.5%	5.9
	Cu	50	7.46
	Cc	0.72	0.71
	USCS	SW-SM	SW
	Description		well graded sand with gravel

Site 2			
Sieve Size	Sieve Opening (mm)	2B	2D
7 cm	70	99%	-
6 cm	60	96%	-
4 cm	40	-	98%
"5/8 in"	15.875	47%	53%
"5/16 in"	7.9375	33%	67%
# 4	4.75	28%	72%
# 10	2	19%	81%
# 20	0.84	11%	89%
# 40	0.425	8%	92%

# 60	0.25	6%	94%
# 100	0.15	4%	96%
#200	0.075	2%	98%
	water content (w)	5.1	18.1
	Cu	26.7	26.00
	Cc	5.9	0.43
	USCS	GW	SW
	Description	well graded gravel	well graded sand with gravel

Site 4				
Sieve Size	Sieve Opening (mm)	4B	4C	4D
-	600		95.00	
-	300	99	-	99
"5/8 in"	15.875	83	25.00	98
"5/16 in"	7.9375	67	20.00	87
# 4	4.75	58	17.00	73
# 10	2	46	13.00	51
# 20	0.84	40	9.00	35
# 40	0.425	37	8.00	29
# 60	0.25	34	6.00	24
# 100	0.15	32	5.00	21
#200	0.075	21	5.00	18
	water content (w)	24.8	11.6	41.1
	Cu	475	100	60.00
	Cc	0.47	1.21	1.67
	USCS		GW-GM	SW-SC
	Description	silty sand	well graded gravel with silt and sand	clayey sand with gravel

Site 5			
Sieve Size	Sieve Opening (mm)	5-U	5-L
6 cm	60	-	99%
3 cm	30	98%	-
"5/8 in"	15.875	82%	66%
"5/16 in"	7.9375	67%	47%
# 4	4.75	57%	33%
# 10	2	40%	18%
# 20	0.84	25%	18%
# 40	0.425	18%	7%
# 60	0.25	13%	4%
# 100	0.15	9%	3%
#200	0.075	6%	2%
	water content (w)	23%	8%
	Cu	31.7	17.50
	Cc	1.1	3.21
	USCS	SW-SM	GW
	Description	well graded sand with silt and gravel	well graded gravel with sand

Site 7							
Sieve Size	Sieve Opening (mm)	7-3	7-9	7-14	7-FS	7S	7A
7.5 cm	75	-	-	-	-	-	99%
7 cm	70	99%	-	99%	-	-	-
5 cm	50	-	-	97%	-	-	
"5/8 in"	15.875	62%	92%	69%	-	-	45%
"5/16 in"	7.9375	47%	83%	55%	-	-	32%
# 4	4.75	40%	76%	47%	99%	100%	25%
# 10	2	28%	58%	32%	96%	100%	16%
# 20	0.84	15%	40%	17%	96%	100%	7%
# 40	0.425	10%	30%	10%	93%	98%	3%

# 60	0.25	7%	20%	5%	91%	70%	2%
# 100	0.15	5%	12%	3%	78%	23%	1%
#200	0.075	3%	7%	1%	31%	4%	1%
	water content (w)	8%	26%	10%	25%	15%	3%
	Cu	53.57	8.67	25			8.33
	Cc	1.15	0.93	0.81			0.85
	USCS	GW	SW-	SW			GW
	Description	well graded gravel with sand		well graded sand with gravel			well graded gravel with sand

Site 8				
Sieve Size	Sieve Opening (mm)	8B-2	8C	8F
3 cm	30	99%	-	-
"5/8 in"	15.875	76%	85%	69%
"5/16 in"	7.9375	62%	74%	50%
# 4	4.75	49%	65%	42%
# 10	2	39%	48%	31%
# 20	0.84	22%	32%	23%
# 40	0.425	7%	21%	16%
# 60	0.25	3%	14%	12%
# 100	0.15	2%	9%	9%
#200	0.075	1%	5%	4%
	water content (w)	5%	44%	13%
	Cu	18.75	13.89	63.89
	Cc	0.48	1.25	1.74
	USCS	SW	SW-SM	GW-SW
	Description	well graded sand with gravel	silty sand	

10.0 Appendix B

Site Descriptions, See Fig. 3 for site locations

10.1 Site 1

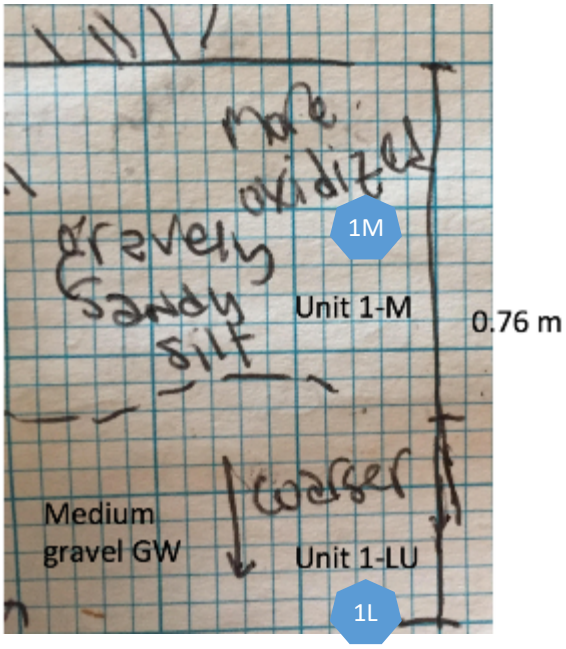

Site 1 is located on Seventeen Creek Ice Contact Complex above the CRLC. The hole was 2 m deep. Two units were observed and the contact between the units is gradational and undulates slightly

Unit 1-M is a medium-loose hard, subangular to rounded well sorted silty sand with gravel (SW-SM). The unit is oxidized near the surface.

Unit 1L is weakly stratified, greenish gray, very loose density, subrounded to rounded, well sorted gravely sand (SW). This unit coarsens downward.

10.2 Site 2

Site 2, located at the very terminal toe of Landslide 28, was the first test pit opened, under saturated conditions. In this pit, Unit A is modern topsoil. Unit B is a brownish gray loose to medium dense rounded to subrounded gravel (GM) with slight silt.

Unit C is an orangish brown loose, subrounded to angular sandy gravel. The contact between unit B and C is undulating.

10.3 Site 4

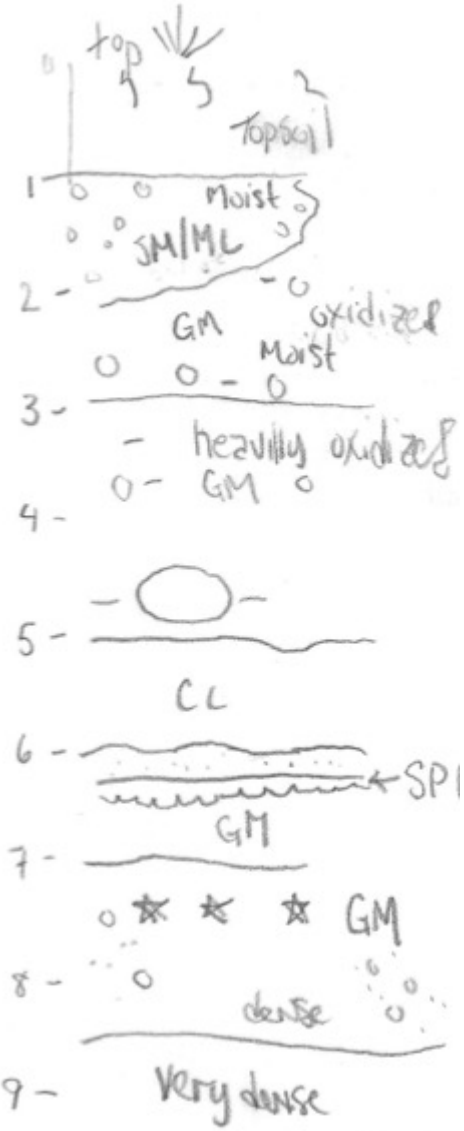

Field Site 4 was located along the old railroad grade along the southern lateral levee of Landslide 28. All observed units are wet, however two days of precipitation preceded fieldwork.

Unit A is topsoil with black organic material and modern roots, speculated that it is mixed with manganese nodules

Unit B (SM/ML in figure) is a very dense, silty sand. Unit grades out to the sides (lens).

Unit C (between 2 and 5 ft in figure) oxidation increases downward and interpreted as the landslide area. Carbon was found near the base. Unit is orangish brown with pockets of detrital organics.

Below 6ft is Unit D. Unit's density increases greatly. At 6ft, at the base of lacustrine unit, slickensides found in the clay.

10.4 Site 5

Site 5 is located along the 50 road between slides 28 and 21. Two units were observed in the test pit and the contact is well defined.

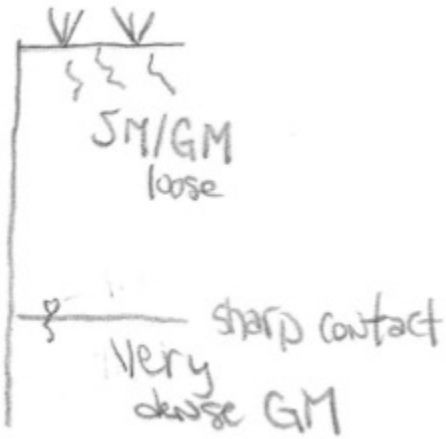

Unit 5-UL is 75 cm deep. It has no bedding or layering and is loose to medium hardness. The unit is brownish well graded sand with silt and gravel (SW-SM). This unit could be colluvium. Modern roots penetrate the entirety of this unit. There is slight seepage at the base of this unit.

Unit 5-LL is a very dense greenish gray, very dense and moist subangular to subrounded well graded sand with gravel (GW).

10.5 Site 7

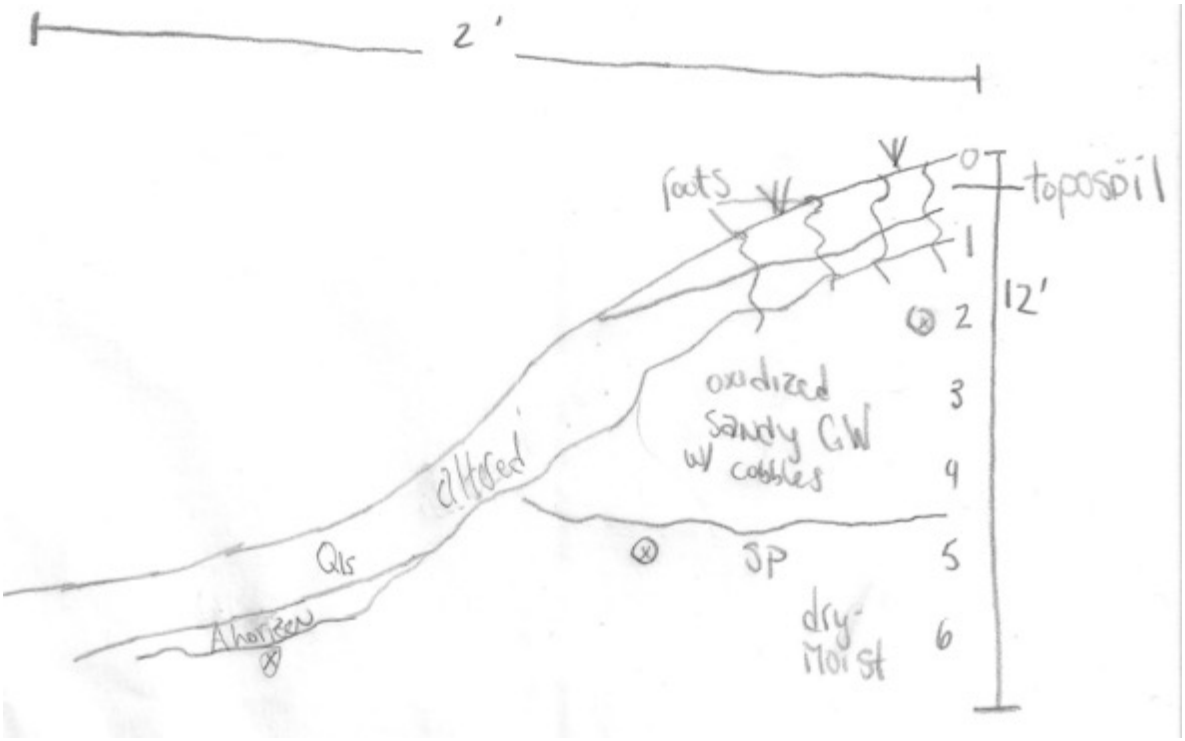

10.6 Site 8

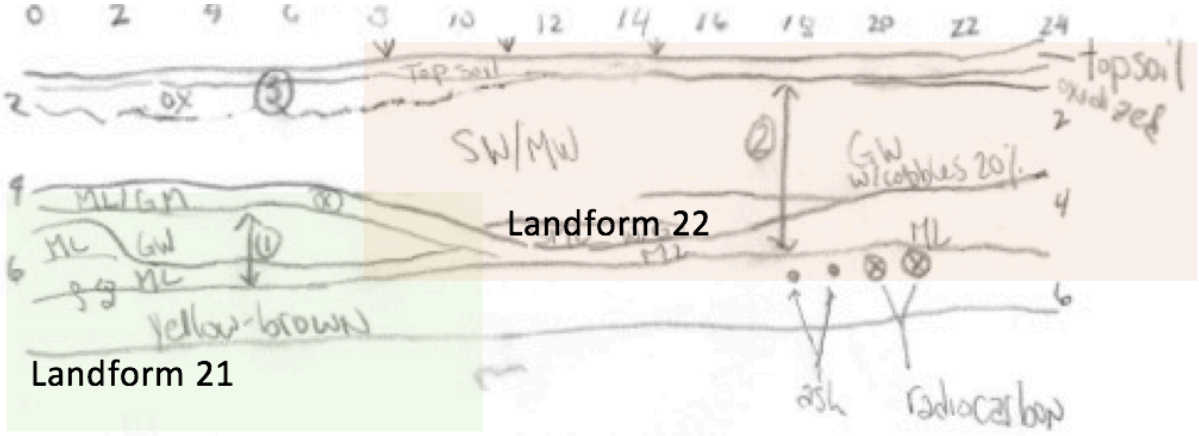

1. Oldest landslide at site
2. Separate landslide from unit 1.
3. Interpreted as a remobilization of unit 2.

10.7 Site 10

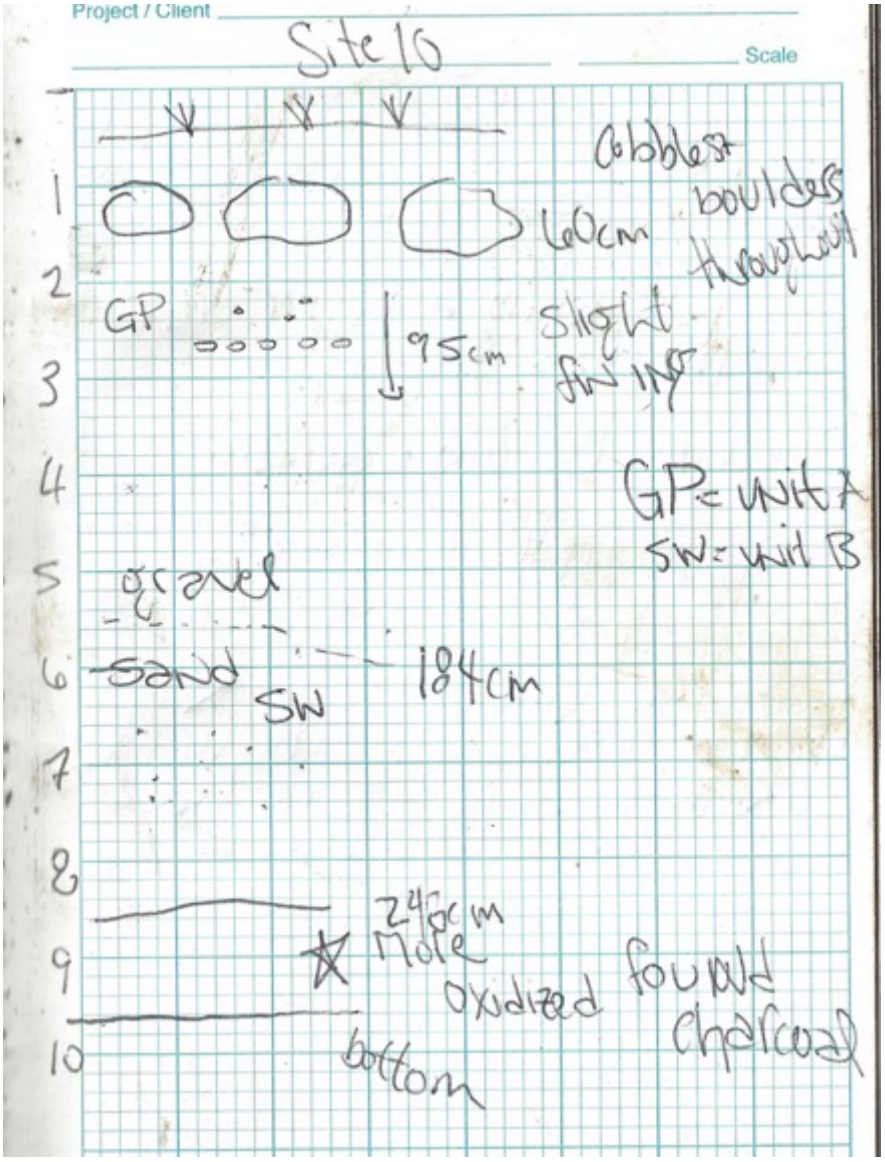

No A horizon found at this site, only C horizons, where three charcoal samples were found. The contact between sand and gravel at 184 cm is irregular. Possible weak bedding in the gravel and boulders is observed. Pit was very unstable.

11.0 Appendix C

Mineralogy

Sample	Mineral	Percentage
2B	Quartz	40
	Granitic lithics	30
	Metamorphosed, greenish lithics	20
	Kyanite	10
2D	Garnet-rich lithics	15
	Quartz	30
	Granitic Lithics	40
	Calcite	5
5-UL	Red, weathered lithics	5
	Mica (light colored)	5
	Greenish, metamorphic lithics	50
	Garnet	20
1-LU	Granitic lithics	40
	Greenish, metamorphic lithics	20
	Reddish lithics	10
4D- difficult to sample	Reddish lithics	10
	Granitic lithics	10
4B	Metamorphic (micaceous) lithic	10
	quartz	30
	Reddish lithic	10
	Granitic lithics	30
4C	Glacial ‘clods’	40
	Reddish lithics	5
	Granitic lithics	20
	quartz	20
7A-UU	Granitic lithics	20
	Quartz	20
	Metamorphic lithics	10
	Reddish lithics	5
7-3	Quartz	30
	Metamorphic lithics	20
	Granitic lithics	30
	Reddish Lithics	5

12.0 Appendix D

Mobility Indices

Landslide Site	H(m)	L (m)	H:L	L/H	Area (km)	Volume (m^3) (Guzzeti et al 2009)	Density kg/m^3
Cedar 28	212.35	952.7	0.22	4.49	0.49	1.32E+07	247.24
30	212.19	1076.8	0.20	5.07	0.64	1.94E+07	247.24
32	51.17	194.5	0.26	3.80	0.01	4.67E+04	247.24
33	210.82	572.4	0.37	2.72	0.33	7.43E+06	247.24
27	186.89	1020.1	0.18	5.46	0.42	1.05E+07	247.24
26	172.89	320.8	0.54	1.86	0.15	2.37E+06	247.24
25	174.94	648.5	0.27	3.71	0.29	6.16E+06	247.24
22	88.33	527.1	0.17	5.97	0.09	1.13E+06	247.24
23	130.29	251.8	0.52	1.93	0.08	9.52E+05	247.24
21	194.95	888.2	0.22	4.56	0.36	8.43E+06	247.24
Oso LS (Iverson et al 2015)	190.00	2000	0.10	10.5	0.94		2000

LS#	H (m)	g (m/s)	Seismic velocity	Density (kg/m^3)	Volume (m^3) Guzzeti et al	ρgVH
28	212.35	9.8	1158.24	0.25	1.56E+09	8.03E+11
30	212.19	9.8	1158.24	0.25	2.74E+09	1.41E+12
32	51.17	9.8	1158.24	0.25	4.36E+05	5.41E+07
33	210.82	9.8	1158.24	0.25	6.80E+08	3.47E+11
27	186.89	9.8	1158.24	0.25	1.13E+09	5.11E+11
26	172.89	9.8	1158.24	0.25	1.30E+08	5.43E+10
25	174.94	9.8	1158.24	0.25	5.18E+08	2.20E+11
22	88.33	9.8	1158.24	0.25	4.42E+07	9.48E+09
23	130.29	9.8	1158.24	0.25	3.45E+07	1.09E+10
21	194.95	9.8	1158.24	0.25	8.16E+08	3.86E+11